Stem Cell Reports
Article
ISSCR
OPEN ACCESS

Generation of innervated cochlear organoid recapitulates early development of auditory unit

Mingyu Xia,[1,2] Jiaoyao Ma,[1,2] Mingxuan Wu,[1,2] Luo Guo,[1,2] Yan Chen,[1,2] Geng-lin Li,[1,2] Shan Sun,[1,2] Renjie Chai,[6,7,8,9,*] Huawei Li,[1,2,3,4,5,*] and Wenyan Li[1,2,3,4,*]

[1]ENT Institute and Otorhinolaryngology Department of Eye & ENT Hospital, State Key Laboratory of Medical Neurobiology and MOE Frontiers Center for Brain Science, Fudan University, Shanghai 200031, PR China
[2]Institutes of Biomedical Sciences, Fudan University, Shanghai 200032, China
[3]NHC Key Laboratory of Hearing Medicine (Fudan University), Shanghai 20003, China
[4]The Institutes of Brain Science and the Collaborative Innovation Center for Brain Science, Fudan University, Shanghai 200032, China
[5]Shanghai Engineering Research Centre of Cochlear Implant, Shanghai 200031, China
[6]State Key Laboratory of Bioelectronics, Department of Otolaryngology-Head and Neck Surgery, Zhongda Hospital, School of Life Sciences and Technology, Jiangsu Province High-Tech Key Laboratory for Bio-Medical Research, Southeast University, Nanjing 210096, PR China
[7]Co-Innovation Center of Neuroregeneration, Nantong University, Nantong 226001, PR China
[8]Institute for Stem Cell and Regeneration, Chinese Academy of Science, Beijing, PR China
[9]Beijing Key Laboratory of Neural Regeneration and Repair, Capital Medical University, Beijing 100069, PR China
*Correspondence: renjiec@seu.edu.cn (R.C.), hwli@shmu.edu.cn (H.L.), wenyan_li@fudan.edu.cn (W.L.)
https://doi.org/10.1016/j.stemcr.2022.11.024

SUMMARY

Functional cochlear hair cells (HCs) innervated by spiral ganglion neurons (SGNs) are essential for hearing, whereas robust models that recapitulate the peripheral auditory circuity are still lacking. Here, we developed cochlear organoids with functional peripheral auditory circuity in a staging three-dimensional (3D) co-culture system by initially reprogramming cochlear progenitor cells (CPCs) with increased proliferative potency that could be long-term expanded, then stepwise inducing the differentiation of cochlear HCs, as well as the outgrowth of neurites from SGNs. The function of HCs and synapses within organoids was confirmed by a series of morphological and electrophysiological evaluations. Single-cell mRNA sequencing revealed the differentiation trajectories of CPCs toward the major cochlear cell types and the dynamic gene expression during organoid HC development, which resembled the pattern of native HCs. We established the cochlear organoids with functional synapses for the first time, which provides a platform for deciphering the mechanisms of sensorineural hearing loss.

INTRODUCTION

Organoids provide promising platforms for disease modeling, drug discovery, and therapeutical strategy establishment (Sun et al., 2021; Wang et al., 2021). Due to the immense self-organizing capacity of stem cells in vertebrates, a wide variety of organoids from tissue-specific stem/progenitor cells or pluripotent stem cells (PSCs) have been generated to recapitulate some of the original aspects of the tissue organization, cellular composition, and function of organs, including the brain, intestine, liver, and lung (Basak et al., 2017; Huch et al., 2015; Lancaster et al., 2013; Nichane et al., 2017). However, most organoids represent only a specific part of the target organ, and they have severe limitations in modeling disorders or diseases involving interactions between distinct functional regions. Thus, a more comprehensive strategy, such as integrating different areas or vascularization, would enable organoid cells to better achieve functionalization (Giandomenico et al., 2019; Homan et al., 2019; Tao et al., 2021).

Inner ear organoids have been induced stepwise from human or mouse PSCs in three-dimensional (3D) culture (Koehler et al., 2013, 2017). They harbor a layer of tightly packed hair cells (HCs) (Koehler et al., 2017; Liu et al., 2016) that closely resemble the structural and biochemical characteristics of the vestibular HCs that are responsible for the sensation of head movement and gravity, rather than cochlear HCs that are responsible for sound detection. The lack of cochlear HCs in inner ear organoids derived from PSCs might be because of missing cues from the cochlear compartment or the complicated assortment of local inductive signals during inner ear development.

The tissue-specific stem cells, or progenitors, serve as another resource for generating cochlear organoids. We previously defined the residing stem cells from the adult mouse vestibular sensory epithelium (Li et al., 2003), and studies have also shown that cells with proliferative capacity can be isolated from the cochlea, and that these proliferative progenitor cells are Wnt-responsive LGR5$^+$ supporting cells (SCs) (Bramhall et al., 2014; Shi et al., 2012). Although, unlike the stem cells/progenitors from other epithelial tissues, such as the intestine, LGR5$^+$ cochlear progenitors cannot effectively expand and replace lost HCs. They can be induced to a limited proliferative state under specific conditions *in vivo* (Li et al., 2015; Shi et al., 2012). The factors used in previous conditions for inner ear organoid culture from LGR5$^+$ progenitors provide essential but inadequate cues for long-term propagation of LGR5$^+$ CPCs

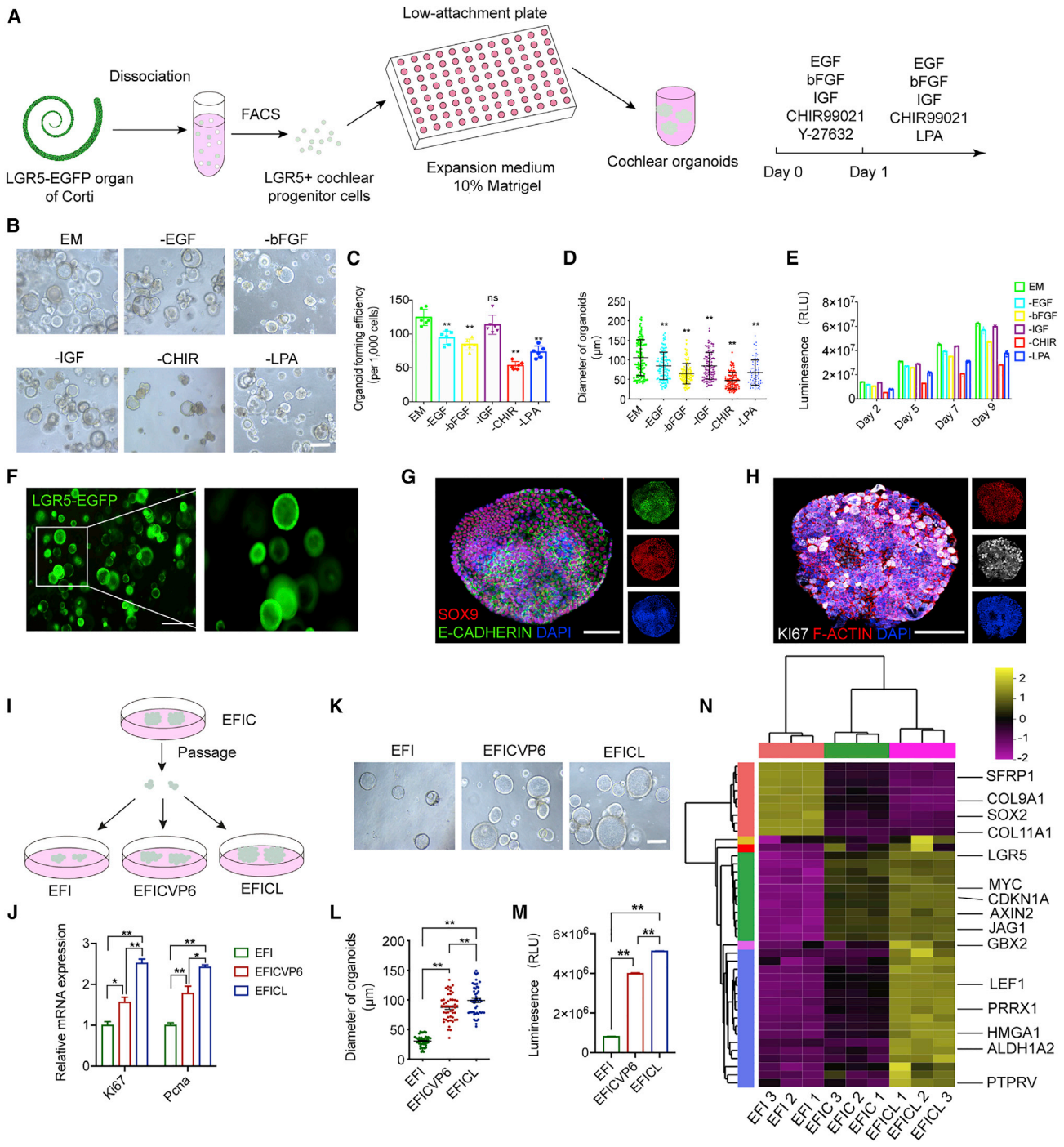

Figure 1. Generation of cochlear organoids from single CPCs in the chemical-defined culture system

(A) A schematic of the experimental strategy for generating cochlear organoids from CPCs.

(B) Representative bright-field images of cultured organoids (P0) from single CPCs under the indicated conditions. Scale bar, 150 μm.

(C) Quantifying organoid-forming efficiency under the indicated conditions (n = 6 independent experiments). The data are presented as means ± SEM. $^{**}p < 0.01$, $^{ns}p \geq 0.05$ (one-way ANOVA followed by Tukey's multiple comparisons test).

(D) Quantification of organoid size in different media. Each dot represents an organoid. 96–101 organoids at each condition, three independent experiments. The data are presented as means ± SEM. $^{**}p < 0.01$ (one-way ANOVA followed by Tukey's multiple comparisons test).

(legend continued on next page)

(McLean et al., 2017; Kubota et al., 2021). Meanwhile, there is no evidence that CPC-derived organoids recapitulate the morphological, transcriptomic, or functional characteristics of cochlear compartments using the currently available protocols.

During the inner ear development, a signal from the adjacent auditory spiral ganglion induced the timing of terminal mitosis of sensory HC precursors and their subsequent differentiation (Bok et al., 2013). Considering the essential role of spiral ganglion neurons (SGNs) in shaping the micro-environment of the cochlear compartment, neuron-innervated organoids from cochlear progenitors might better achieve the maturation and functionalization of organoid HCs. Furthermore, establishing functional synapses in the organ of Corti is pivotal for the perception of auditory signals (Johnson et al., 2009; Safieddine et al., 2012). Generating the cochlear organoids with functional peripheral synaptic connections within this co-culture system will benefit the understanding of morphological, physiological, and molecular characteristics of the HC synaptic machinery, which is critical to auditory perception.

In the current study, we screened multiple compounds and growth factors to generate comprehensive cochlear organoids that integrate the sensory HCs and transmission neurons. With the new culture system, we identified more HCs within the innervated organoids that resembled the features of cochlear HCs, a portion of which could form functional synapses with neurons. Meanwhile, single-cell mRNA sequencing revealed that the differentiation trajectories of CPCs recapitulate the early development of cochleae. Thus, we developed the cochlear organoids with functional synapses for the first time, which can be used for modeling the sensorineural hearing loss caused by the degeneration of both HCs and synapses *in vitro*.

RESULTS

Optimized culture condition for the expansion of cochlear progenitor cells

To identify the optimal condition to enhance the expansion of CPCs, we systematically screened factors that target several key signaling pathways during development, including the Wnt, Shh, BMP4, and Hippo pathways (Bok et al., 2013; Chai et al., 2012; Gnedeva et al., 2020; Li et al., 2005). Based on the medium containing epidermal growth factor (EGF), basic fibroblast growth factor (bFGF), and insulin-like growth factor (IGF) (EFI) for sorted CPCs, we found that CHIR99021 (CHIR) (a glycogen synthase kinase-3 inhibitor for Wnt signaling activation) combined with lysophosphatidic acid (LPA) (one of the essential bioactive phospholipids) allowed for the highest organoid formation capacity (Figures S1A–S1F). Y-27632, a Rho kinase inhibitor, has been verified to promote the survival of dissociated cells (Watanabe et al., 2007). We found that Y-27632 had a pro-survival effect during days 0–4 in passage (P) 0 (started with single cells) and days 0–1 in P1 (started with organoid fragments) (Figures S1G and S1H). Thus, we established an optimal strategy for increasing the self-renewal capacity of CPCs: during days 0–1, EFI with CHIR and Y-27632 were supplied, maintaining the survival and vitality of fluorescence-activated cell sorting (FACS)-sorted LGR5$^+$ CPCs. Then LPA is included to replace Y-27632 for promoting the self-renewal of CPCs and subsequent cell division (Figure 1A; Video S1). To further assess

(E) Quantification of organoid viability cultured in expansion medium or medium where one specific component was removed (n = 5 independent experiments).
(F) Representative fluorescence images showing the cochlear progenitor cell marker LGR5 expression as indicated by EGFP in P0 organoids (day 8). Scale bar, 500 μm.
(G) Immunofluorescence analysis of P0 organoids at day 8 showing the expression of stem cell marker SOX9 and the epithelial cell marker E-CADHERIN. Scale bar, 50 μm.
(H) Immunofluorescence analysis of organoids at day 8 showing the expression of the proliferative cell marker KI67 and the cytoskeleton protein F-ACTIN. Scale bar, 50 μm.
(I) A schematic of the experimental strategy of comparing the pro-proliferative effect of the three different conditions. EFI refers to EGF, bFGF, and IGF; EFICVP6 refers to EGF, bFGF, IGF, CHIR, VPA, pVc., and 616452; EFICL refers to EGF, bFGF, IGF, CHIR, and LPA.
(J) Real-time PCR analysis showed the relative expression of proliferation-related genes. Results were normalized to GAPDH in the same sample and then normalized to the expansion group (n = 3 independent experiments). The data are presented as means ± SEM. *p < 0.05, **p < 0.01 (one-way ANOVA followed by Tukey's multiple comparisons test).
(K) Representative bright-field images of cultured organoids under the indicated conditions. Scale bar, 100 μm.
(L) Quantification of organoid size in different media. 50 organoids at each condition, three independent experiments. The data are presented as means ± SEM. **p < 0.01 (one-way ANOVA followed by Tukey's multiple comparisons test).
(M) Luminescent cell viability assay measuring CPCs cultured in the indicated conditions (n = 3 independent experiments). The data are presented as means ± SEM. **p < 0.01 (one-way ANOVA followed by Tukey's multiple comparisons test).
(N) Heatmap of inner ear gene expression determined by mRNA sequencing of organoids cultured in the three conditions: essential expansion medium alone, + CHIR, and + CHIR + LPA (n = 3 independent experiments).

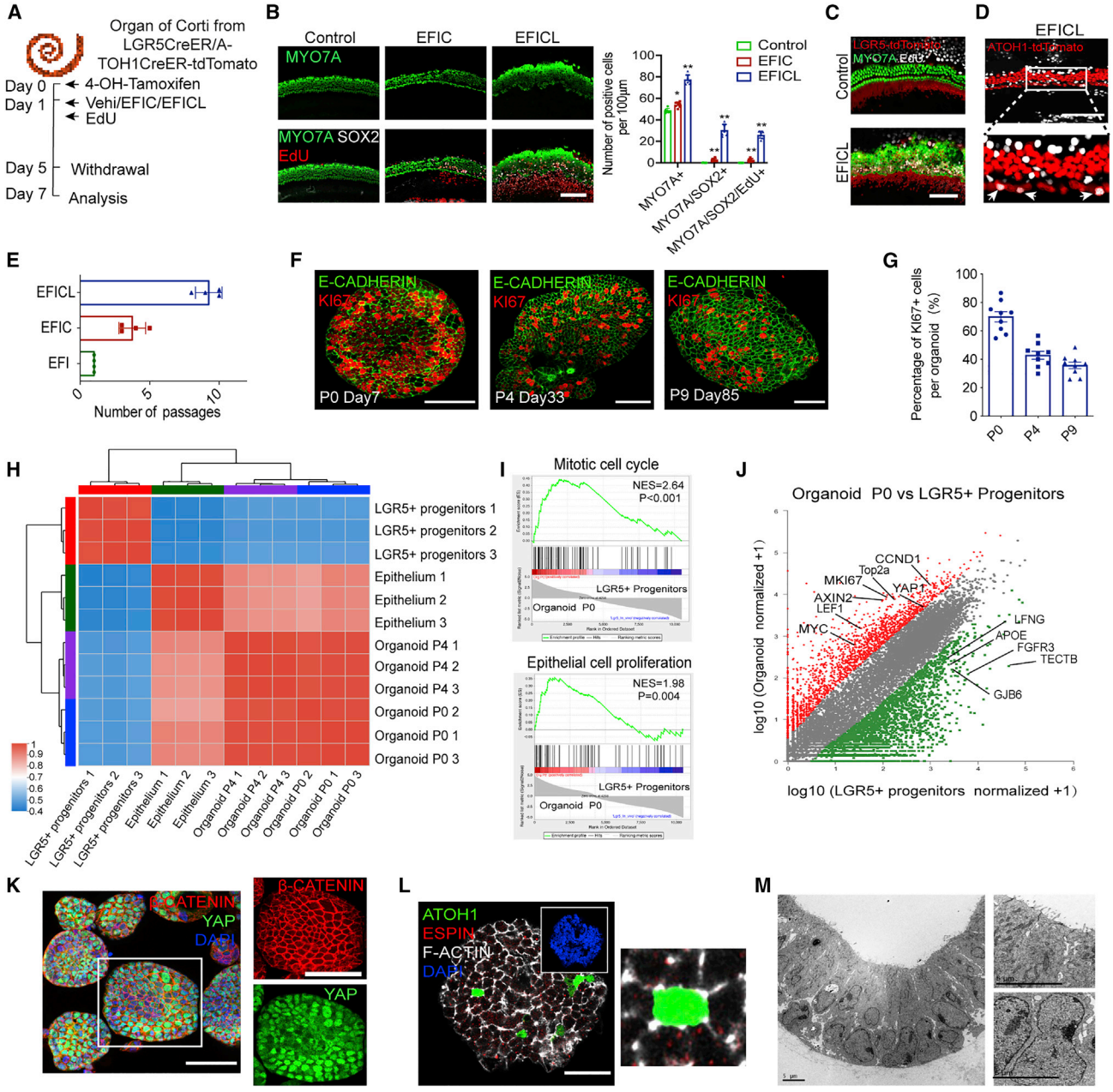

Figure 2. The regenerative effect of the expansion components and characterization of the stably expanded organoids

(A) A schematic of the experimental strategy of the regenerative effect of the expansion medium.

(B) Representative fluorescence images showing MYO7A, SOX2, and 5-Ethynyl-2′-deoxyuridine (EdU) staining of cochlear epithelium treated with vehicle, EFIC, or EFICL. Scale bar, 100 μm. Quantification of the number of MYO7A, MYO7A$^+$/SOX2$^+$, and MYO7A/SOX2$^+$/EdU$^+$ cells in the indicated treatments. n = 6 cochlear explants at each condition, three independent experiments. The data are presented as means ± SEM. *p < 0.05, **p < 0.01 (one-way ANOVA followed by Tukey's multiple comparisons test).

(C) Confocal images showing MYO7A and EdU staining, along with LGR5-tdTomato, in cochleae treated with vehicle or EFICL. Scale bar, 100 μm.

(D) Confocal images showed EdU staining, along with ATOH1-tdTomato, in cochleae treated with EFICL. Scale bar, 100 μm.

(E) Quantification of the passage number of organoids cultured in the indicated medium (n = 4 independent experiments).

(F) Immunofluorescence analysis of passage 0 (day 7), passage 4 (day 33), and passage 9 (day 85) organoids showed the expression of KI67 and E-CADHERIN. Scale bar, 50 μm.

(legend continued on next page)

the requirement of each component in the expansion medium for CPC proliferation, we individually removed every ingredient on day 1, which resulted in a decreased number and size of organoids and reduced cell viability after 10 days of culture, especially withdrawing CHIR (Figures 1B–1E). The results indicate that each component is essential for organoids' optimal formation from LGR5$^+$ CPCs. Meanwhile, we verified that typical markers for epithelial progenitor cells, including LGR5, SOX9, and E-CADHERIN, were sustained in the robust proliferating CPC-derived organoids (Figures 1F–1H).

Then we compared the proliferative capacities of CPCs in our expansion medium with that in the "7F" medium (McLean et al., 2017). Passaged CPCs cultured in the medium containing EGF, bFGF, IGF, and CHIR (EFIC) were transferred into the medium containing EFI, new combinations (EGF, bFGF, IGF, CHIR, and LPA [EFICL]), and "7F" (EGF, bFGF, IGF, CHIR, valproic acid [VPA], 2-phospho-L-ascorbic acid [pVc], 616452) (Figure 1I). We observed that CPCs in our expansion medium acquired significantly increased proliferative ability, which was indicated by the enhanced expression of proliferative markers (Figure 1J), increased size of organoids (Figures 1K and 1L), and augmented cell viability (Figure 1M).

We further investigated the effect of the additional ingredients in the CPC expansion medium on the transcriptome signature of cultured LGR5$^+$ progenitor cells. According to the results from microarray analysis, multiple markers for SCs (*SFRP1*, *COL9A1*, *COL11A1*, and *SOX2*) were downregulated by CHIR, which indicates that dedifferentiation processes were involved in the enhanced expansion of LGR5$^+$ progenitors *in vitro* (Figure 1N). Meanwhile, the markers for progenitors (*LGR5*, *AXIN2*, and *MYC*), as well as some critical genes for inner ear development (*GBX2*, *PRRX1*, *HMGA1*, *ALDH1A2*, and *PTPRV*), were further upregulated by the combination of CHIR and LPA, which indicates that the combination reprogrammed LGR5$^+$ progenitors into a relatively earlier stage.

The enhanced proliferative capacity and extended passages of CPCs

We evaluated the effects of our new expansion medium EFICL on the more physiologically relevant inner ear tissue (Figure 2A). After 4 days of EFICL treatment, the mitotic HC regeneration of cochlear explants abundantly indicated by the increased MYO7A$^+$ total HCs, MYO7A$^+$/SOX2$^+$ young HCs, and MYO7A$^+$/SOX2$^+$/EdU$^+$ new HCs from the proliferation of LGR5$^+$ progenitor cells (Figures 2B and 2C). Remarkably, with another innate HC tracing model, ATOH1-tdTomato mice, we identified that some innate inner hair cells (IHCs) re-entered the cell cycle and incorporated EdU (Figure 2D), which provided the first piece of evidence that the innate HCs could also be activated into the proliferative status with those potent compounds.

We next cultured CPCs in the expansion system under series passages. We confirmed that no apparent organoids were formed from LGR5$^-$ cells after 10 days in the expansion conditions (Figures S2A and S2B). The LGR5$^+$ progenitor cells were expanded and passaged every 8–10 days at a ratio of 1:6–1:8. We noticed that CHIR and LPA could significantly increase the survival time and passage number of LGR5$^+$ progenitors to about 3 months and nine passages. Organoids maintained the epithelial property during the long-term culture (Figures 2E–2G and S2C).

We further evaluated the genetic stability during passages, and the cochlear organoids clustered more closely with E-CADHERIN$^+$ sensory epithelium instead of the sorted LGR5$^+$ progenitors. The transcriptomes of P0 and P4 organoids were highly similar (Figures 2H and S2D), which indicated that the organoids maintain gene stability during early passages. Compared with the sorted LGR5$^+$ progenitors, the expression levels of 5,997 genes were significantly changed in the organoids with a fold change ≥ 5 ($p \leq 0.05$). Gene set enrichment analysis (GSEA) revealed the significant enrichment of genes involved in epithelial cell proliferation, sensory organ development, and stem cell maintenance in the organoids (Figures 2I and S2E). The proliferation-associated genes, such as *MKI67*, *CCND1*, *MYC*, *TOP2A*, and *YAP1*, and the Wnt

(G) Quantification of KI67$^+$ cells of different passage organoids from (F) (nine organoids at each condition, three independent experiments).

(H) A correlogram of the transcriptomes of the indicated cell types was analyzed by Pearson's correlation coefficient (n = 3 independent experiments).

(I) GSEA of differentially expressed genes in organoids at passage 0 versus primary Lgr5$^+$ progenitor cells.

(J) Scatterplot showing differential gene expression comparing passage 0 organoids and primary LGR5$^+$ CPCs based on fold change ≥ 5 and $p \leq 0.05$). Red plots indicate significantly upregulated genes, and green plots indicate significantly downregulated genes.

(K) Immunofluorescence analysis of passage 0 organoids on day 8 showing the expression of YAP and β-CATENIN. Scale bar, 50 μm.

(L) Immunofluorescence analysis of passage 0 organoids showing the expression of ATOH1 and the HC bundle markers ESPIN and F-ACTIN. Scale bar, 50 μm.

(M) Transmission electron microscopy analysis of organoids in expansion medium with microvilli, nuclear fission, and plentiful mitochondria. No stereocilia-like protrusions were found. Scale bars, 5 μm.

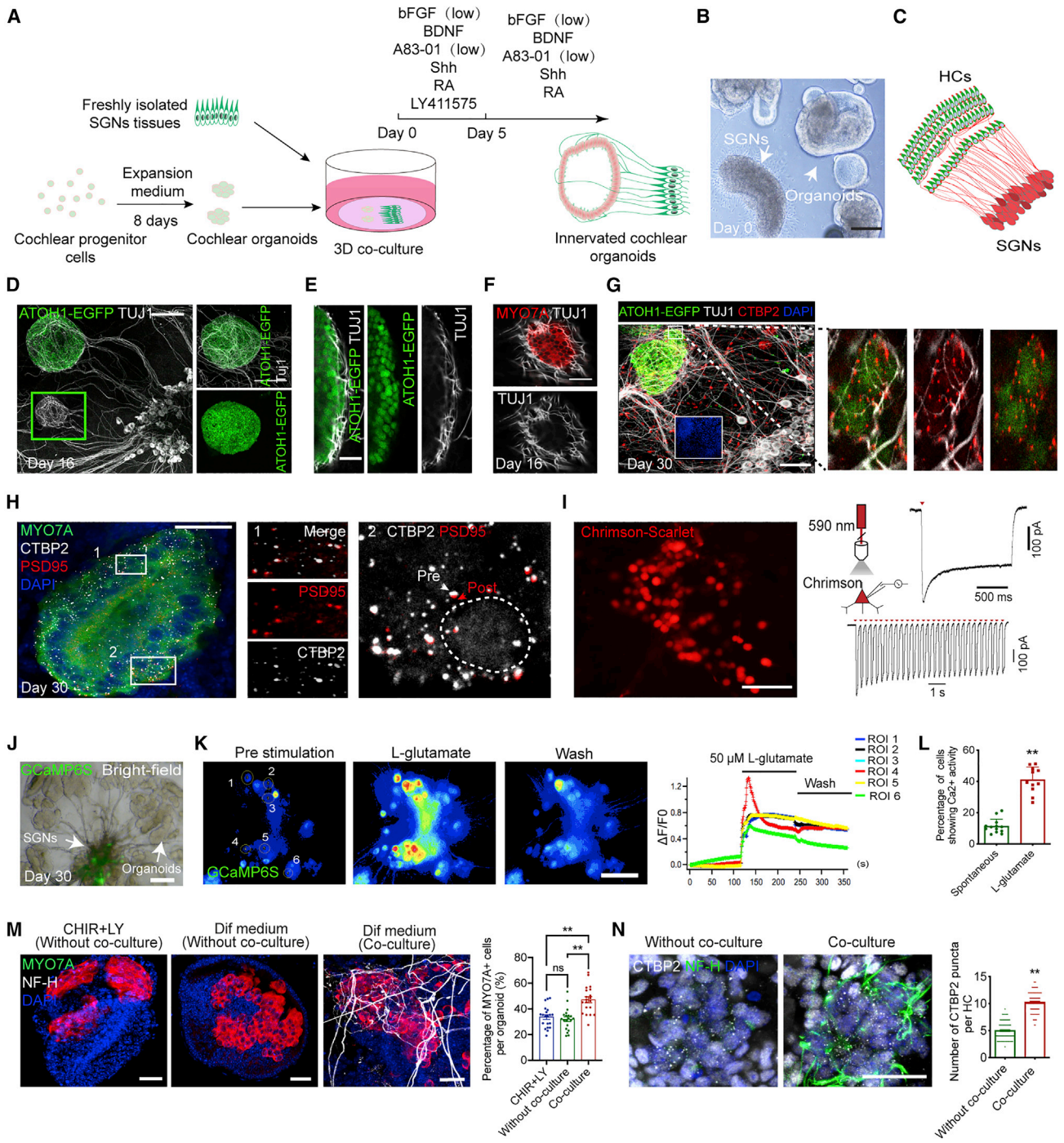

Figure 3. Generating SGN-innervated cochlear organoids with functional auditory circuits

(A) A schematic of the experimental strategy for generating SGN-innervated cochlear organoids by 3D co-culture of cochlear organoids and SGNs.

(B) Bright-field image of co-cultured organoids and SGNs at day 0. Scale bar, 100 μm.

(C) Schematic representation of the peripheral auditory circuit where HCs in the cochlear epithelium connect with SGNs.

(D) Fluorescence images of the co-culture system showed the innervation of ATOH1$^+$ organoid HCs by tracts from TUJ1$^+$ SGNs at day 16. Scale bar, 100 μm.

(E) Higher magnification of the HC region shows the TUJ1$^+$ SGN neurites in contact with ATOH1$^+$ HCs. Scale bar, 25 μm.

(legend continued on next page)

signaling genes (*AXIN2* and *LEF1*) were upregulated in organoids (Figure 2J). In contrast, the marker genes of SC subsets (*LFNG*, *FGFR3*, *APOE*, *TECTB*, and *GJB6*) were significantly downregulated. Immunofluorescence analysis confirmed the high expression of YAP (a Hippo pathway effector) and β-CATENIN (a Wnt pathway effector) in the cultured organoids (Figure 2K). These results suggest that LGR5$^+$ progenitor cells were partially reprogrammed into an epithelial stem cell-like status with higher proliferative potency, which might be partly attributed to the activation of the Wnt and YAP signaling.

We observed a few ATOH1-EGFP$^+$ cells from the organoids cultured in the expansion medium (Figure S2F), a small portion of which also expressed MYO7A without F-ACTIN or ESPIN-labeled stereocilia (Figures 2L and S2G). Transmission electron microscopy showed only microvilli at the apical surface protruding into the lumen (Figure 2M). The prominent nuclei with nuclear fission, plentiful mitochondria, and tight junctions further confirmed the absence of differentiated structures in the organoid cells.

Establishing a staging 3D co-culture system for generating the innervated organoids with function

To fully mimic the auditory unit *in vitro*, we screened multiple factors for inducing the differentiation of cochlear HCs, promoting the survival and outgrowth of neurites, and forming functional synapses simultaneously in a cochlear organoid and neuron co-culture system. Notch inhibition is the dominant strategy for inducing the differentiation of HCs (Li et al., 2015; Roccio et al., 2018), and we found that LY411575 (LY), a γ-secretase inhibitor, could generate numerous MYO7A$^+$ cells and trigger apoptosis, while the side effect could be alleviated by 10 ng/mL bFGF (Figures S3A–S3C). In addition, we found that bone morphogenic protein 4 (Bmp4), retinoic acid (RA), and LY could promote the differentiation of progenitors into HCs with an F-ACTIN-labeled stereocilia structure (Figures S3D–S3E). Meanwhile, we identified that Shh, transforming growth factor β1 (TGF-β1), and RA could also facilitate the survival of dissociated SGNs and promote the outgrowth of neurites based on bFGF and brain-derived neurotrophic factor (BDNF). At the same time, LY, a decisive promoting factor for HC differentiation, could significantly reduce the survival of dissociated SGNs (Figures S4A–S4C). Unlike the dissociated neurons, the neurite growth of cultured SGNs from primary tissue was arrested by TGF-β1 but significantly promoted by A83-01 (Figures S4D and S4E). Based on the results, we defined an optimal staging *in vitro* co-culture system, which started with a cocktail of bFGF, BDNF, Shh, A83-01, RA, and LY during the initial 5 days, then removed LY in the subsequent culture (Figure 3A).

We observed that SGNs could survive up to 60 days in the optimized co-culture medium, and the length of neurites could reach 4.59 ± 0.1 mm after 30 days of culture (Figures S4F and S4G). In the co-culture system, the expanded organoids and the freshly dissected SGNs from the modiolus of post-natal mice were seeded at 100- to 300-μm intervals in a Matrigel droplet (Figure 3B). Like the peripheral auditory circuit (Figure 3C), we observed

(F) Immunofluorescence analysis showed that TUJ1$^+$ neurites surrounded the MYO7A$^+$ HCs. Scale bar, 25 μm.

(G) Representative fluorescence images of co-cultures at day 30 showing TUJ1$^+$ SGN axon projections into ATOH1$^+$ HCs with CTBP2$^+$ presynaptic vesicles (left) and higher magnification of the SGN terminals of the selected region in contact with CTBP2$^+$ presynaptic vesicles (right). Scale bar, 50 μm.

(H) Representative fluorescence images showing the presence of CTBP2$^+$ presynaptic vesicles and PSD95$^+$ postsynaptic vesicles in the MYO7A$^+$ HCs (left). Scale bar, 25 μm. Higher magnification of the HC region showing the CTBP2$^+$ presynaptic vesicles co-localized with PSD95$^+$ postsynaptic vesicles (right). The circle represents the localization of HCs.

(I) Fluorescence microscopy images of SGNs transfected with adeno-associated virus (AAV) DJ-Chrimson-Scarlet. Scale bar, 50 μm. The right representative images showed the red light-induced spiking traces of SGNs at 5 mW/mm^2.

(J) Bright-field and fluorescence microscopy image of co-cultured organoids and SGNs at day 30. SGNs transfected with AAV 2/9-hSyn-GCaMP6S. Scale bar, 100 μm.

(K) Representative calcium imaging of SGNs in co-cultures at day 30. Scale bar, 100 μm. The single-cell tracings of the region of interest (ROI). Time is shown in seconds (s).

(L) Quantification of the percentage of firing SGNs on day 30 of SGN-innervated cochlear organoids under spontaneous conditions or after L-glutamate treatment (11–13 co-cultures at each condition, four independent experiments). The data are presented as means ± SEM. $^{**}p < 0.01$ (t test).

(M) Immunofluorescence analysis of organoids at day 30 stained with MYO7A and neurofilament-H (NF-H) in the three different culture conditions. Scale bar, 25 μm. Quantification of the percentage of MYO7A$^+$ cells per organoid. 20 organoids at each condition, three independent experiments. The data are presented as means ± SEM. $^{**}p < 0.01$, $^{ns}p \geq 0.05$ (one-way ANOVA followed by Tukey's multiple comparisons test).

(N) Immunofluorescence analysis of organoids at day 30 stained with CTBP2 and NF-H in the three different culture conditions. Quantification of the number of CTBP2$^+$ presynaptic vesicles per HC from single cultured organoids and co-cultures at day 30. 100 HCs from 8–12 organoids at each condition, three independent experiments. The data are presented as means ± SEM. $^{**}p < 0.01$ (t test).

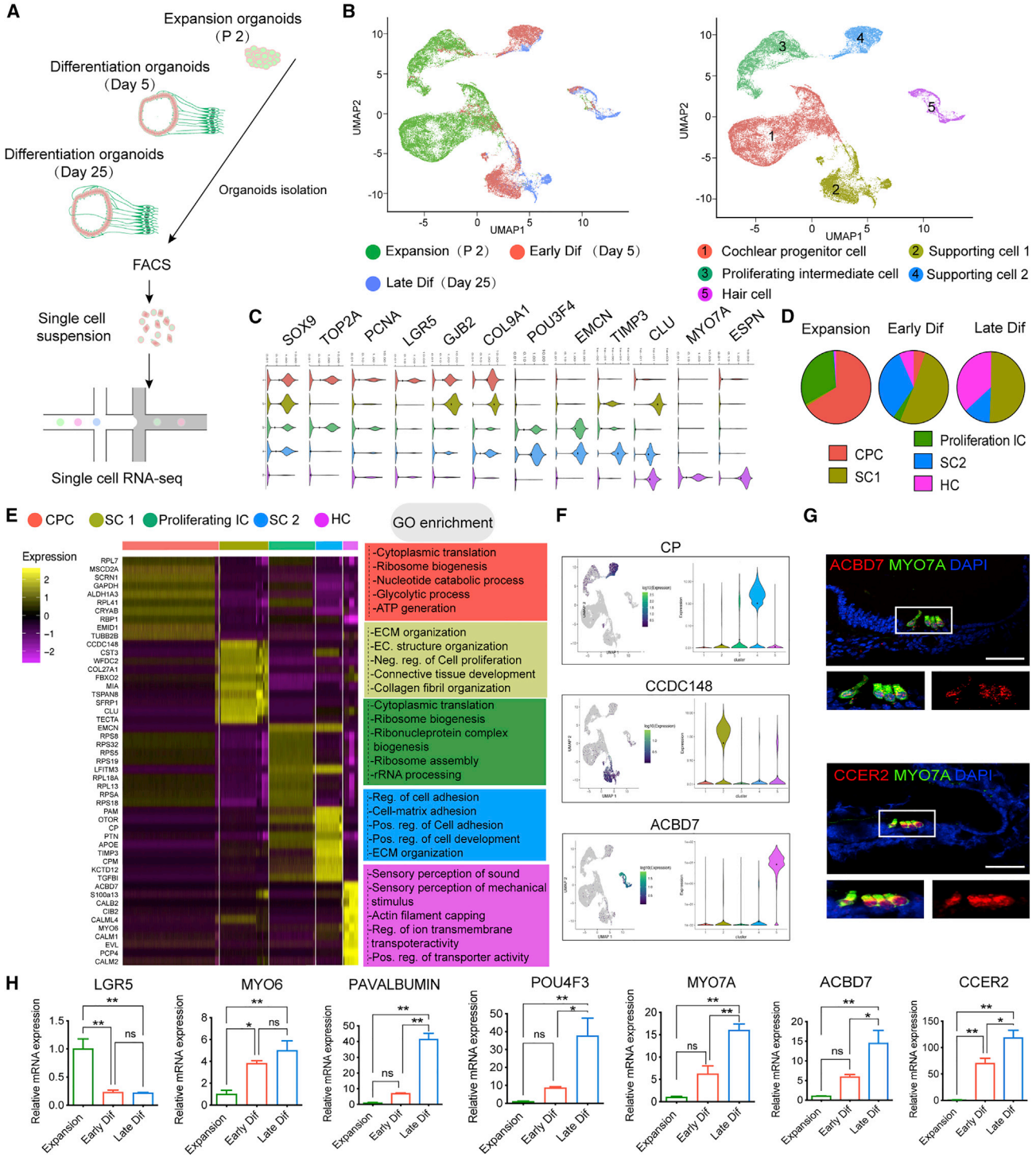

Figure 4. Single-cell RNA-seq (scRNA-seq) reveals the main cell types of cochlear epithelium during organoid development

(A) Overview of the scRNA-seq of cochlear organoids at different stages.

(B) The scRNA-seq datasets from P2 organoids cultured in the expansion medium were integrated with the differentiated day 5 and day 25 organoid datasets and projected onto UMAP plots. Colors denote the five main cell clusters from three different time points.

(C) Violin plots showing the expression of representative genes across the five main clusters.

(D) The proportion of cells from each cluster in the indicated stages.

(legend continued on next page)

that TUJ1$^+$ neurites from the co-cultured neurons grow toward the differentiated organoids and form physical attachments with the newly generated ATOH1-EGFP$^+$ and MYO7A$^+$ HCs on the surface of organoids at day 16 (Figures 3D–3F). After 30 days of co-culture, presynaptic puncta marked by CTBP2 were detected on the surface of ATOH1$^+$ HCs and were highly correlated with the distribution of neurites (Figure 3G; Video S2). Further, we detected the paired localization of the CTBP2 and the postsynaptic marker PSD95 in the neurite-innervated HCs (Figure 3H).

The function of SGNs and the newly formed synapses in this novel co-culture system was further evaluated. We recorded the channelrhodopsin Chrimson-mediated spikes of light-triggered action potentials under stimulation with 590 nm red light stimulation by the whole-cell clamp (Figure 3I) and observed the significantly increased transient Ca^{2+} activity indicated by a genetically encoded calcium reporter (GCaMP6s) (Figure 3J) in the SGNs after the treatment of 50 mM KCl (Figure S4H). We also confirmed that long-term co-cultured neurons maintain excitability through electrophysiological assessments (Figures S4I–S4L). HCs release glutamate at ribbon synapses to excite postsynaptic SGNs via glutamate receptors to relay auditory information to the CNS (Martinez-Monedero et al., 2016). We observed significantly increased electrical activity in neurons instantly after the administration of L-glutamate after 30 days of co-culture (Figure 3K; Video S3). Compared with the spontaneously firing neurons, the percentage of firing neurons under L-glutamine stimulation was significantly increased (Figure 3L), which further demonstrates functional synapses were formed between HCs and SGNs. We compared the yield of HCs within organoids cultured in our differentiation medium, with or without neurons, and the organoids cultured in the previously published conditions with the existence of CHIR and LY (McLean et al., 2017). We observed significantly more HCs in the current co-culture system (Figure 3M). Meanwhile, more presynaptic puncta were identified within the HCs after co-culture with neurons (Figure 3N).

Single-cell transcriptional profiles during the development of co-cultured organoids

To gain insight into the cell-type specification and transcriptional profiles during the development of the epithelium compartment of the co-cultures, we performed single-cell RNA sequencing (scRNA-seq) on the collected organoids in expansion medium, early differentiation (5 days after co-culture), and late differentiation (25 days after co-culture) (Figure 4A). Using uniform manifold approximation and projection (UMAP), unsupervised clustering of the combined dataset of 46,814 total cells was divided into five distinct clusters (Figure 4B). Based on lineage-specific markers, we annotated the five clusters as follows: cochlear progenitor cell (CPC), supporting cell 1 (SC1), proliferating intermediate cell (proliferating IC), supporting cell 2 (SC2), and HC (Figures 4B and 4C). As differentiation progressed, dynamic changes in cell proportion were noticed (Figure 4D).

The heatmap showed that in CPC and proliferating IC populations, the most uniquely expressed genes were *ALDH1A3*, *LFITM3*, and ribosome biogenesis-associated genes (such as *RPL7* and *RPS8*) (Figure 4E). The HC population highly expressed HC genes, such as *CALB2*, *CIB2*, *MYO6*, and *PCP4*. Gene Ontology (GO) analysis showed the characteristic function enrichment of each cell type. Apart from the known genes, we found some potential markers for each cell type, such as *CP* and *CCDC148* for SCs and *ACBD7* and *CCER2* for HCs (Figures 4F and S5A). We also verified potential new HC markers, *ACBD7* and *CCER2*, whose mRNAs were uniquely expressed in HCs of the cochlear epithelium (Figure 4G). Real-time PCR revealed the gradually decreased expression of *LGR5* and increased expression of the HC marker genes, such as *MYO6* and *POU4F3*, during organoid development (Figure 4H).

The developing HC within co-cultured organoid captures the early cochlear HC gene dynamic

Because transcription factors (TFs) are vital regulators determining cell fate, we identified cell-type-specific TFs with enriched expression in the developing organoids (Figure 5A), such as *CEBPD*, *LEF1*, and *MYC*, were highly expressed in cycling CPCs. In contrast, the HC cluster strongly expressed *TAL1*, *ZEB1*, *GATA2*, *SIX2*, etc. The Slingshot program revealed three different trajectories during CPC differentiation to elucidate the fate transition of the CPCs (Figures S5B and S5C). Along the HC trajectory, the heatmap revealed gene expression changed progressively from cycling progenitor cells to differentiated HCs (Figure S6D). Meanwhile, we clustered HCs and identified

(E) Heatmap showing the most highly expressed genes of the five main clusters. Each gene group's GO enrichment analysis results are displayed to the right.

(F) Visualization showing the expression of potential marker genes for clusters 2, 4, and 5.

(G) RNA-scope analysis of ACBD7 and CCER2 mRNA expression of the P2 cochlear epithelium. HCs were stained for MYO7A. Scale bar, 50 μm.

(H) Real-time PCR analysis showed the relative expression of HC-related genes. Results were normalized to GAPDH in the same sample and then normalized to the expansion group (n = 3 independent experiments). The data are presented as means ± SEM. *p < 0.05, **p < 0.01, $^{ns}p \geq 0.05$ (one-way ANOVA followed by Tukey's multiple comparisons test).

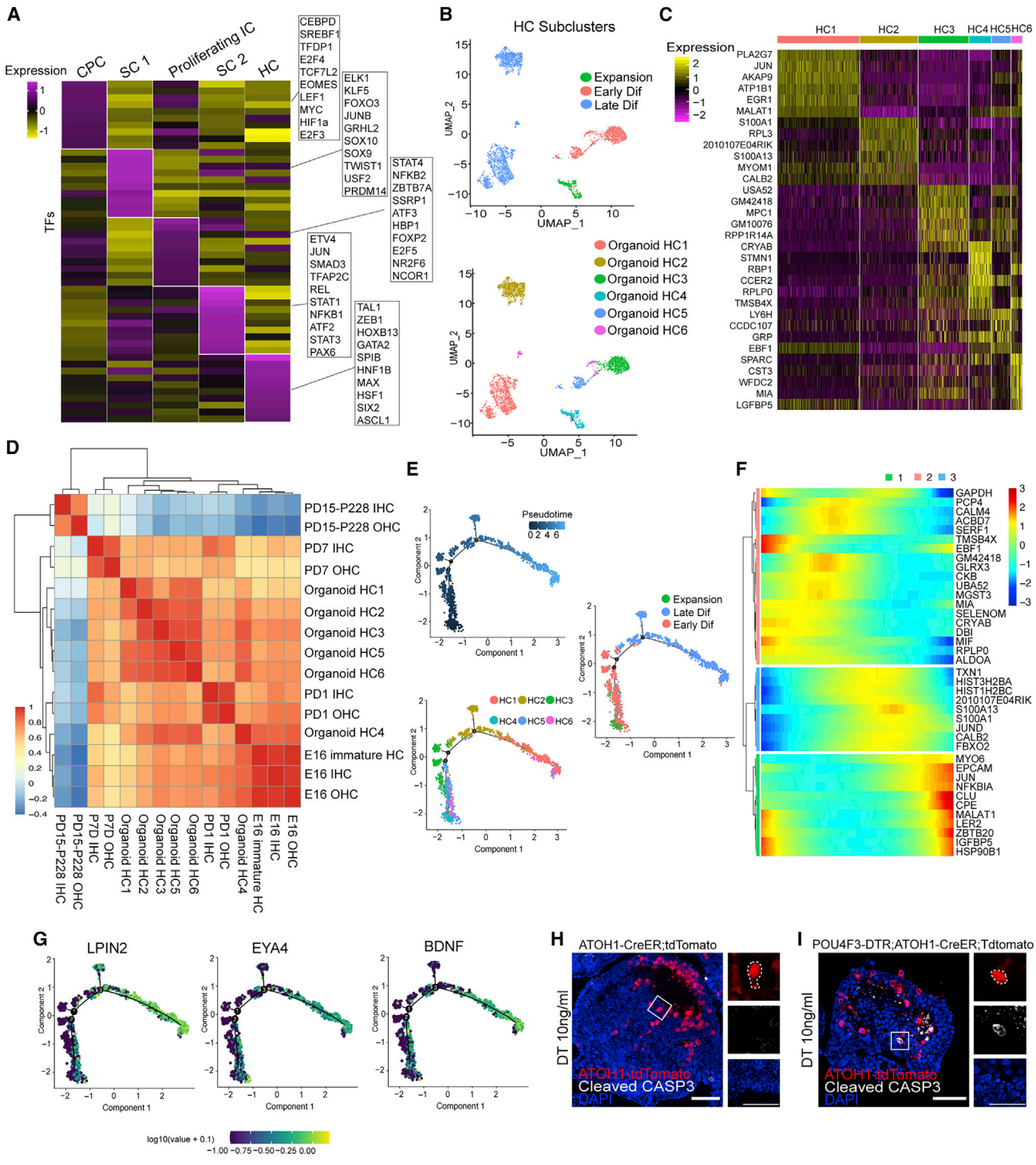

Figure 5. The genetic profile of developing organoid HC is similar to the cochlear HC during early development

(A) Heatmap showing expression of representative TFs differentially expressed among organoid clusters.

(B) UMAP plots showing six HC subtypes of the three time points.

(C) Heatmap showed the expression signature of the top six genes in each HC subtype.

(D) Pearson's correlation coefficient analyzed a correlogram for transcriptomes of the *in vitro* organoid HCs and the *in vivo* cochlear HCs.

(E) Lineage trajectory of the organoid HC sub-cluster by pseudotime of different states.

(F) Heatmap showed three distinct groups of genes with dynamic expression patterns along the pseudotime.

(legend continued on next page)

six distinct HC sub-populations (Figure 5B). Among those clusters, we noticed that *TMSB4X*, expressed in young HCs during development (Zhu et al., 2019), was significantly enriched in the expansion and early-differentiation-stage-dominated HC clusters (clusters HC4 and HC6) (Figure 5C). Clusters HC1 and HC2 were occupied by late differentiation organoids, which expressed specialized HC genes, such as *PLA2G7* and *CALB2* (Kolla et al., 2020). To compare gene expression profiles of organoid HCs with the *in vivo* cochlear HCs, we analyzed the correlation of six sub-cluster organoid HCs, embryonic day (E) 16 to post-natal day (PD) 7 cochlear HCs (Kolla et al., 2020), and PD15–P228 cochlear HCs (Ranum et al., 2019) by Pearson's correlation coefficient (Figure 5D).

Beyond the status of organoid HCs indicated by the correlogram, we investigated the maturation of organoid HCs by Monocle 2 (Figure 5E). Similar to the Slingshot program of HC differentiation trajectory, genes are known to be enriched in mature HCs, such as *MYO6* and *ESPN*, which displayed a time-dependent increase as pseudotime progressed (Figures 5F and S5D). We also noticed the dynamic expression of HC markers, such as *PCP4*, *CIB2*, and *ACBD7*, along the trajectory (Figures 5F and S5E). Notably, dynamic changes in multiple genes related to the functional maturation of HCs were also observed over pseudotime, including the increased expression of the K^+-channel-related genes *ATP1B1* and *CACNA1D*, as well as the dynamic changes in the expression of Ca^{2+}-channel-associated genes *CALM4*, *CALB2*, and *CIB2*, which were all consistent with the changes in K^+ and Ca^{2+} currents that occur in cochlear HCs during development (Figure S5E) (Beurg et al., 2008). During the organoid HC maturation, the outer hair cell (OHC) marker *LPIN2*, Na^+/K^+-ATPase regulator *EYA4*, and genes involved in synapse formation, such as *BDNF*, were increased along the timeline (Figure 5G). These results indicate that the transcriptome feature of organoid HCs recapitulates the developing cochlear HCs of early stages *in vivo*.

Mutations in numerous genes responsible for cochlear proteins are the leading cause of sensorineural hearing impairment (Shearer et al., 2011). Analysis of deafness-related gene expression in differentiated day 25 organoids of the HC and SC types showed that the cell-type specificity related to auditory genetic disease was preserved in the organoids (Figure S5F). To test the application of the auditory circuit, we developed cochlear progenitors from transgenic $POU4F3^{+/DTR}$ mouse, a selectively ablated HC for investigating the HC regeneration mouse model (Cox et al., 2014), in the co-cultures. After adding *diphtheria toxin* (DT), we observed apoptosis specifically in the lineage-traced $ATOH1^+$ HCs in the organoids from $POU4F3^+$/DTR; ATOH1CreER-tdTomato mice (Figures 5H and 5I). These indicated that the innervated organoids might be used as a model for HC regeneration.

HCs in co-cultures recapitulate the morphological and electrophysiological profile of post-natal cochlear HCs

We further studied the morphology and function of HCs in co-cultured organoids. Among the ATOH1-$tdTomato^+$ cells from co-cultured organoids, 4.88% ± 1.72% exclusively expressed VGLUT3, a specific maker for IHCs from PD7 (Li et al., 2018); 45% ± 4.28% exclusively expressed PRESTIN, which was uniquely expressed in cochlear OHCs from PD0 (Belyantseva et al., 2000); and 50.86% ± 5.47% $tdTomato^+$ HCs expressed both VGLUT3 and PRESTIN at day 30 (Figures 6A–6C). Furthermore, stereocilia-like structures were labeled by F-ACTIN and ESPIN (Figures 6D and 6E) and confirmed by the transmission electron microscope (Figure S6A).

A prominent kinocilium surrounded by a cluster of cilia and microvilli was observed from the organoids after 6 days of co-culture, while a shorter kinocilium with a larger cluster of compact stereocilia located in a larger cuticular plate was identified on day 12 (Figure 6F). After 30 days, the kinocilium could no longer be identified, and the stereocilia in the organoids were arranged in a V or C shape with tip links between adjacent stereocilia. The dynamic changes in the bundle-like structures of organoids simulated the morphological transition of cochlear HC bundles during development (Tilney et al., 1992; Zine and Romand, 1996).

The majority of the $MYO7A^+$ HCs at day 30 could take up FM1–43 (Figure S6B). Electrophysiological recordings were performed to more precisely assess the electrical properties of the $tdTomato^+$ organoid HCs (Figure S6C). Voltage-dependent inward Na^+ currents with voltage-dependent activation were found in organoid HCs at day 30 (Figure 6G), and these could also be detected in immature cochlear HCs at the post-natal stage (Oliver et al., 1997). To further characterize the identity and maturation of organoid HCs, we analyzed the K^+ currents in HCs at different time points during the differentiation step. Voltage-dependent outward K^+ currents in the HCs at day 30 were triggered by depolarizing voltage steps from the holding potential of −80 mV, which resembled the magnitude of the

(G) Expression levels of representative genes along the HC lineage trajectory.
(H) Fluorescence images of the apoptotic cell marker Cleaved-CASP3 staining and tdTomato in cochlear organoids derived from ATOH1-CreER; tdTomato mice after DT treatment. Scale bar, 50 μm.
(I) Fluorescence images of Cleaved-CASP3 staining and tdTomato in cochlear organoids derived from POU4F3-DTR; ATOH1-CreER; tdTomato mice after DT treatment. Scale bar, 50 μm.

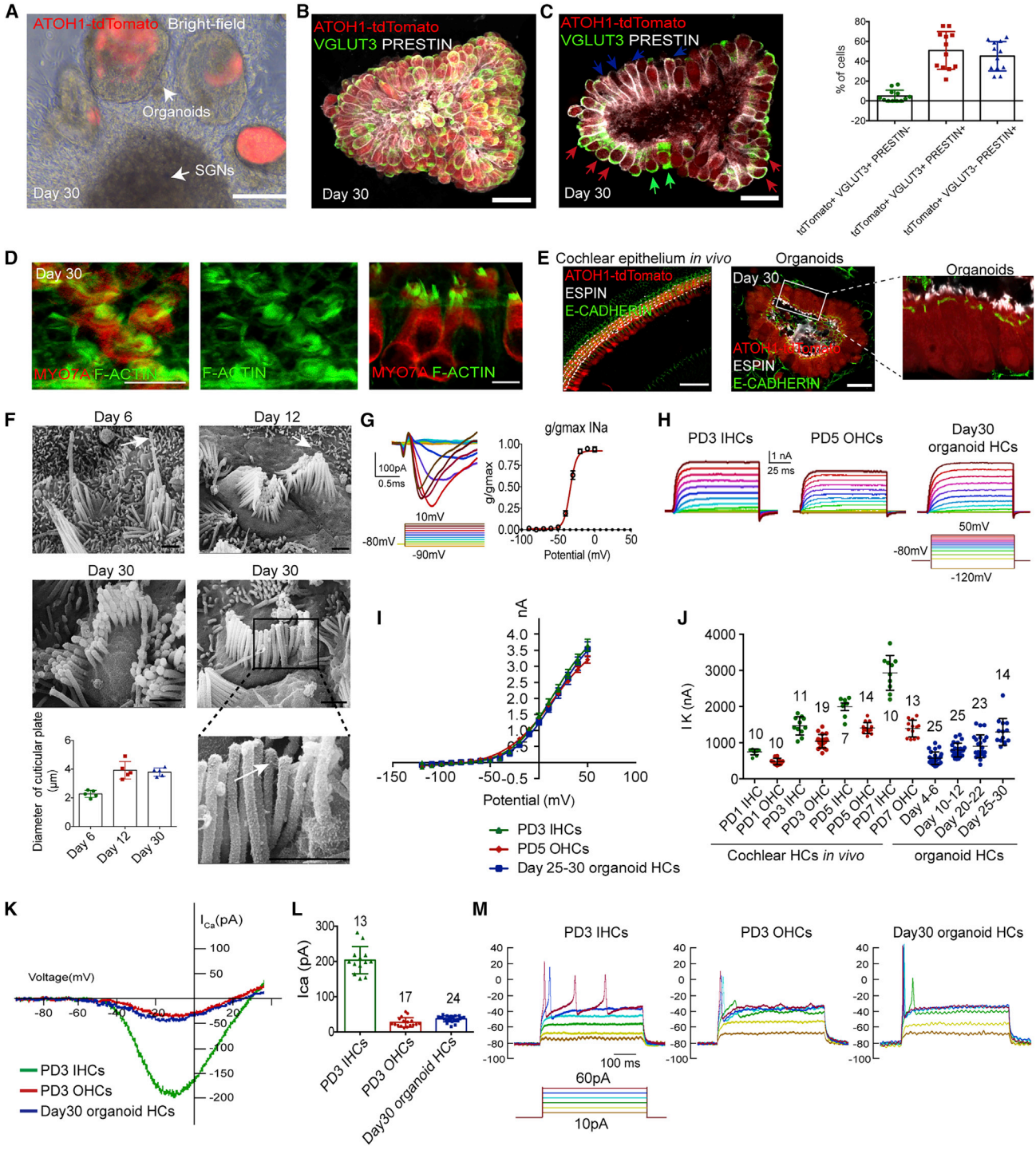

Figure 6. HCs in organoids recapitulate the morphological and electrophysiological profile of post-natal cochlear HCs

(A) Bright-field and fluorescence microscopy image of innervated organoids at day 30. Atoh1-tdTomato indicated the generated HCs. Scale bar, 100 μm.

(B) Immunofluorescence images of whole-mount staining of IHC marker VGlut3 and the OHC marker PRESTIN (3D reconstruction) of co-cultured cochlear organoids at day 30. Scale bar, 25 μm.

(legend continued on next page)

PD3 IHCs and PD5 OHCs (Figures 6H and S6D). The steady-state values of the outward K^+ currents of the day 25–30 organoid HCs were measured to generate current-voltage (*I-V*) curves, and these were highly similar to those of native PD3 IHCs and PD5 OHCs (Figure 6I). The development of outward K^+ currents over time in neonatal IHCs, OHCs, and organoid HCs is shown in Figures 6J and S6E. We found that the gradually increased current in the developing organoid HCs reached a value at 0 mV of 1.3 ± 0.1 nA at days 25–30. The development patterns of K^+ currents resembled those of post-natal cochlear HCs (Figure 6J). We further blocked outward K^+ currents by using CsCl and TEA-Cl in the internal solution to isolate Ca^{2+} currents, and the I_{Ca}-V curves indicated that Ca^{2+} currents of day 30 organoid HCs were activated at around −60 mV and reached a maximum at −10 mV, which resembled those of PD3 OHCs (Figure 6K). Interestingly, the peak amplitude of Ca^{2+} currents of the organoid HCs (36.95 ± 1.72 pA) was much lower than that of the native PD3 IHCs (203.3 ± 10.68 pA) (Figure 6L), and it was comparable with the OHCs at PD3, a developmental stage when Ca^{2+} currents are at their maximum amplitude (Beurg et al., 2008). Action potentials are thought to be essential for HC maturation (Jeng et al., 2020), and no spontaneous action potential firing was seen in organoid HCs (data not shown). We recorded fired spikes from organoid HCs responding to stepped current injections that resembled PD3 OHCs (Figure 6M), which indicated that organoid HCs tend to differentiate into OHC. Taken together, the cochlear organoid HCs were found to be functional and followed a similar development pattern as post-natal cochlear HCs.

DISCUSSION

In this study, we described an optimized protocol to generate innervated cochlear organoids that possess the major cell types of cochlear sensory epithelia and functional HC-SGN circuits. First, CPCs gained enhanced proliferative capacity in the optimal expansion medium. They were reprogrammed into a relatively earlier stage of progenitors and could be long-term expanded under series passages by activating Wnt and YAP signaling (Chai et al., 2012; Gnedeva et al., 2020; Xia et al., 2020). Second, the co-culture system achieved a balance between the differentiation of HCs and the outgrowth of neurites, and neurons promoted the formation of cochlear HCs and reached functional synapses with HCs. In addition, we dissected the characteristic of organoid HC and the regulatory mechanism of HC development through scRNA-seq, electrophysiological, and morphological analysis, which suggested innervated organoids as a reliable model for studying inner ear development and sensorineural hearing loss.

We observed that some innate IHCs re-entered the cell cycle and incorporated EdU, whereas more reliable Cre

(C) Immunofluorescence analysis (z stack projection) and quantification of organoids showing the expression of VGLUT3 and PRESTIN. The green arrow indicates $VGLUT3^+/PRESTIN^-$ cells, the red circle indicates $VGLUT3^+/PRESTIN^+$ cells, and the blue arrow indicates $VGLUT3^-/Prestin^+$ cells. Scale bar, 25 μm. 12 organoids, three independent experiments.

(D) Immunofluorescence images showing $MYO7A^+$ HCs and $F\text{-}ACTIN^+$ hair bundles of the differentiated day 30 organoids. The scale bar represents 10 μm.

(E) Fluorescence images of E-CADHERIN staining, ESPIN-stained stereocilia-like protrusions, and $ATOH1\text{-}tdTomato^+$ HCs in the cochlear epithelium (left) and cochlear organoids (right). Scale bar, 50 μm.

(F) Scanning electron microscopy showed the morphology of the hair bundles of cochlear organoids at different stages and quantified the diameter of the cuticular plate of the HCs. Five HCs from two organoids at each stage, two independent experiments. The arrow indicates the kinocilium. Scale bar, 1 μm.

(G) Family of Na^+ currents of differentiated day 30 organoid HCs evoked by the depolarizing steps shown below, fitted by a Boltzmann equation (line) with a half-maximal activation voltage of −34 mV.

(H) Examples of outward K^+ currents for PD3 IHCs and PD5 OHCs from mouse cochleae, and day 30 organoid HCs evoked by the voltage protocol are below.

(I) Steady-state IK^+-V curves for the current traces showing the current-voltage relationship for PD3 IHCs (n = 11), PD5 OHCs (n = 14), and day 25–30 organoid HCs (n = 14). HCs from five to seven cochlear explants or organoids, three to five independent experiments.

(J) Peak outward K^+ current (evoked by 0 mV) for native HCs (PD1, PD3, PD5, and PD7) and organoid HCs (days 4–6, 10–12, 20–22, and 25–30). The total number of patched cells is indicated in the graph. HCs from five to seven cochlear explants or organoids, three to five independent experiments.

(K) Ca^{2+} current-voltage relations for PD3 IHCs and PD5 OHCs, and day 30 organoid HCs recorded under a voltage clamp in response to a voltage ramp from −90 to +70 mV in 300 ms.

(L) Mean ± SEM peaks of ICa^{2+} for PD3 IHCs, PD5 OHCs, and day 30 organoid HCs. The total number of cells for each stage is indicated above the bars. HCs from six cochlear explants or organoids, three independent experiments.

(M) Representative membrane responses of IHCs (PD3), OHCs (PD3), and organoid HCs (day 30) to step current injections (protocol shown below).

lines were needed to trace the original HC, such as VGLUT3CreER, POU4F3CreER, or GFICreER mouse lines, in order to demonstrate further the proliferation effects of the EFICL cocktail on HCs. In addition, to validate the application of the cocktail in regeneration, we should deliver the cocktail into the inner ear to investigate the effects on cochlear cells *in vivo* in the future.

The single-cell transcriptome atlas of organoids allows for mapping genes to particular cell types to understand the mechanism of cell fate determination (Low et al., 2019; Wu et al., 2018). Our study showed that the transcriptome transition pattern might be more suitable for explaining the fate transition of proliferating progenitor cells in the early E stage and during HC development (Gnedeva and Hudspeth, 2015; Ruben, 1967). Meanwhile, we identified new marker genes for cochlear HCs, such as *ACBD7* and *CCER2*, which were also found in a recent study to be exclusively expressed in HC clusters from post-natal mouse cochleae (Kolla et al., 2020). Notably, the dynamic gene expression of the developing organoid HC provides us with potential clues that promote HC regeneration and maturation.

We observed that the stereocilia bundles of HCs in the epithelial compartment of the co-cultures mimicked the developmental pattern of cochlear HCs, including the dynamic changes to the kinocilium, which is necessary for the initial orientation of the HCs and degenerates as hearing is activated (Tilney et al., 1992; Zine and Romand, 1996). We also found that there were HCs with V- or C-shaped stereocilia after 30 days of differentiation, which was very similar to the bundle morphology of the OHCs and IHCs of the cochlea. Similar to the inner ear organoids generated from PSCs (Koehler et al., 2017), the stereocilia-like extensions of the cochlear organoids were uniformly oriented toward the lumen. Cell polarity formation in organoids might derive from the extrusion of the extracellular matrix-triggered planar cell polarity signaling (Montcouquiol and Kelley, 2020). Although more complicated arrangements of HCs and SCs and the polarity of the organ of Corti were not achieved in our new system, emerging bioengineering strategies might be used to steer the cell composition and their 3D organization.

Consistent with scRNA-seq analysis data, in-depth electrophysiological analysis revealed that the HCs of the organoids could mimic the development pattern of the cochlear HCs up to PD7 *in vivo*. Meanwhile, we noticed that the Ca^{2+} current and action potential of the organoid HCs closely resembled those of native OHCs, which might be because of the majority of $ATOH1^{+}$ HCs being $PRESTIN^{+}$ or $PRESTIN^{+}/VGLUT3^{+}$ OHCs, and only 4.88% of the $ATOH1^{+}$ HCs were similar to IHCs as marked by $ATOH1^{+}/VGLUT3^{+}/PRESTIN^{-}$ (Li et al., 2018). The significant difference in the proportion of two HC subtypes might be because of insufficient induction signals in our culture system. The reason why organoid HCs cannot continue to mature into adulthood-like HCs might be attributed to the following factors: the existing culture system lacked the interaction between HCs and mesenchymal cells, marginal cells, and immune cells. Such interaction-provided lymph ion concentration, immune micro-environment, and physical interactions were not considered in the current system. More efforts should be put into the direct differentiation of CPCs into diverse mature HC or SC subtypes and on mimicking the delicate topological structure of the organ of Corti by applying new biocompatible materials, 3D printing technology, and bioengineering strategies.

Our staging co-culture system facilitates the formation of peripheral auditory circuity between cochlear HCs in organoids and SGNs. During the development of the cochlea, various factors involved in axon guidance have been shown to influence the radial innervation of SGNs, including Wnt9a (Munnamalai et al., 2017), Ephrin-A5/EphA4 (Defourny et al., 2013), and Semaphorin-3F/Neuropilin-2 (Coate et al., 2015). We found that the differentiated organoids could automatically induce the directional outgrowth of neurites toward sites with multiple HCs. In the single-cell analysis of the late-differentiated HC cluster, we identified the high expression of *BDNF*, which encodes the BDNF protein that is critical for sensory neuron survival and the establishment of neuronal projections to sensory epithelia during the development of the inner ear through the interaction with the TRKB receptor of SGNs (Postigo et al., 2002; Wan et al., 2014). The high levels of endogenous BDNF from HCs and exogenous supplementation might serve as one of the pivotal factors for the survival of SGNs and ribbon synapse formation. Moreover, the peripheral auditory circuit in our 3D co-culture system could be maintained for a relatively long period (up to 2 months), which makes it possible to investigate the function of peripheral auditory units related to diverse cell types at different developmental stages.

In conclusion, we developed a protocol for establishing functional cochlear innervated organoids through the timely regulation of multiple signaling pathways related to cochlea development. Our model can be used for deciphering the mechanisms behind the proliferation of CPCs, the specific differentiation of cochlear HCs, and the diversity and functional maturation of synapses between HCs and SGNs. Furthermore, the established peripheral auditory circuit could model cochlear diseases related to sensorineural hearing loss and thus might serve

as a tool for screening drugs or genetic vectors in the cochlea.

EXPERIMENTAL PROCEDURES

Resource availability

Corresponding author

Further information and requests for resources and reagents should be directed to and will be fulfilled by the corresponding author, Wenyan Li (wenyan_li@fudan.edu.cn).

Materials availability

This study did not generate new unique reagents.

Data and code availability

The bulk RNA-seq and scRNA-seq data have been deposited in the Gene Expression Omnibus (GEO) under ID codes GEO: GSE180552 and GSE180553.

The published scRNA-seq datasets of the cochlea were used (GEO: GSE137299 and GSE114157.)

Animal model

LGR5-EGFP-IRES-creERT2 mice (Barker et al., 2007) (stock #008875) and Rosa26-tdTomato mice (Madisen et al., 2010) (stock #007914) were purchased from the Jackson Laboratory. ATOH1-EGFP mice (Helms et al., 2000) were obtained from J. Johnson (University of Texas Southwestern Medical Center, Dallas, TX, USA), ATOH1CreER mice (Chow et al., 2006) were obtained from S. Baker (St. Jude Children's Research Hospital, Memphis, TN, USA), and POU4F3-DTR mice (Golub et al., 2012) were obtained from S. Stone (University of Washington, Seattle, WA, USA). Genotyping of transgenic mice is described in Table S1. All animal experiments were approved by the Institutional Animal Care and Use Committee of Fudan University.

Culture of cochlear epithelia and isolation of mouse primary CPCs

The cochleae were dissected from P0–P1 mice and quickly placed in cold PBS (Hyclone). The modiolus and the stria vascularis were carefully removed to separate the sensory epithelia. The tissues were mounted on the 2 mg/mL laminin-coated glass Petri dishes for cochlear epithelial culture. Details are provided in the supplemental experimental procedures.

Primary CPC culture and expansion

Typically, sorted cells were resuspended in an expansion culture medium with a mixture of ice-cold Matrigel (354230; Corning) at a ratio of 1:10 (v/v) and then seeded in non-attachment plates. Details are provided in the supplemental experimental procedures.

Organoid-forming efficiency and viability assays

To exclude dead cells, we labeled sorted cells by propidium iodide (Sigma) and counted them using a hemocytometer. A 100-μL single-cell suspension (~1,000 cells) mixed with 10 μL Matrigel was plated into an ultra-low-attachment U-bottom 96-well plate (Corning), with each culture condition tested in triplicate. Details are provided in the supplemental experimental procedures.

Organoid-SGN explant co-culture

For organoid differentiation, a glass Petri dish was coated with 2 mg/mL laminin solution (diluted in PBS) overnight. Details are provided in the supplemental experimental procedures.

Immunofluorescence analysis and quantification

The cultured organoids in the expansion medium were collected by centrifugation and fixed with 4% paraformaldehyde (PFA) (Sigma) on ice for 30 min and then centrifuged at 600 rpm for 5 min. Details are provided in the supplemental experimental procedures.

In situ hybridization assays

Cochleae were isolated from P1 mice and fixed in 4% PFA for 6 h at room temperature. Details are provided in the supplemental experimental procedures.

Electron microscopy

Cochlear organoids differentiated at days 6, 12, and 30 were fixed in 2.5% glutaraldehyde and 2% PFA diluted in 0.1 M phosphate buffer (PB) overnight. For scanning electron microscopy, samples were dehydrated in an ethanol gradient after washing in PB. Details are provided in the supplemental experimental procedures.

RNA isolation and quantitative real-time PCR analysis

Organoids in co-cultures were picked and washed with cold PBS and centrifuged to remove the Matrigel. Details are provided in the supplemental experimental procedures.

RNA sequencing and analysis

Organoids cultured in the basic medium (EFG, bFGF, IGF), the basic medium + CHIR, and the basic medium + CHIR + LPA were collected, and P0 and P4 organoids in the expansion medium were collected. Details are provided in the supplemental experimental procedures.

Single-cell sequencing and analysis

Organoids from P2 (day 8) in expansion medium, differentiated at day 5, and differentiated at day 25 were collected and incubated with 0.125% trypsin for 25 min and dissociated into single cells by mechanical pipetting. Details are provided in the supplemental experimental procedures.

Optogenetic stimulation and electrophysiological recordings

The AAV DJ carrying the coding sequences for Scarlet and Chrimson driven by the CAG promoter was generated using a virus-free helper system. Details are provided in the supplemental experimental procedures.

Ca^{2+} imaging

Co-cultured SGNs at day 30 were used for Ca^{2+} imaging. SGNs were transfected with AAV2/9-hSyn-GCaMP6s for 24 h and then exchanged with a fresh medium. Details are provided in the supplemental experimental procedures.

Statistical analyses

Statistical differences were calculated using GraphPad Prism 6.0. Details are provided in the supplemental experimental procedures.

SUPPLEMENTAL INFORMATION

Supplemental information can be found online at https://doi.org/10.1016/j.stemcr.2022.11.024.

AUTHOR CONTRIBUTIONS

H.L., W.L., and R.C. designed the study and wrote the manuscript. M.X. performed most of the experiments, including mouse breeding, cochlear organoid culture, immunofluorescence assay, calcium imaging, scanning electron microscopy, and analysis. J.M. did the electrophysiological recordings, and G.L. provided technical support. M.W. performed the time-lapse imaging and *in situ* hybridization assays. M.X. and L.G. analyzed the mRNA-seq and scRNA-seq data. S.S. and Y.C. helped with the experiment design and manuscript editing. All authors commented on the manuscript.

ACKNOWLEDGMENTS

We thank Guisheng Zhong and Fangzhi Tan of the iHuman Institute, ShanghaiTech University, for help in the construction of AAV-Chrimson. We appreciate the assistance received from Intanx Life (Shanghai) Co. Ltd. for scRNA-seq data processing and consultation. We thank Yalin Huang for her help with the confocal microscope. This work was supported by the National Key R&D Program of China (2017YFA0103900, 2022ZD0205400, and 2021YFA1101300), National Science Foundation for outstanding young people (81922018), National Natural Science Foundation of China (82271170, 81922018, 82192861, 81771011, and 82101239), and Shanghai Sailing Program (21YF1405500).

CONFLICT OF INTERESTS

The authors declare no competing interests.

Received: May 24, 2022
Revised: November 28, 2022
Accepted: November 30, 2022
Published: December 29, 2022

REFERENCES

Barker, N., van Es, J.H., Kuipers, J., Kujala, P., van den Born, M., Cozijnsen, M., Haegebarth, A., Korving, J., Begthel, H., Peters, P.J., and Clevers, H. (2007). Identification of stem cells in small intestine and colon by marker gene Lgr5. Nature *449*, 1003–1007. https://doi.org/10.1038/nature06196.

Basak, O., Beumer, J., Wiebrands, K., Seno, H., van Oudenaarden, A., and Clevers, H. (2017). Induced quiescence of Lgr5+ stem cells in intestinal organoids enables differentiation of hormone-producing enteroendocrine cells. Cell Stem Cell *20*, 177–190.e4. https://doi.org/10.1016/j.stem.2016.11.001.

Belyantseva, I.A., Adler, H.J., Curi, R., Frolenkov, G.I., and Kachar, B. (2000). Expression and localization of prestin and the sugar transporter GLUT-5 during development of electromotility in cochlear outer hair cells. J. Neurosci. *20*, RC116.

Beurg, M., Safieddine, S., Roux, I., Bouleau, Y., Petit, C., and Dulon, D. (2008). Calcium- and otoferlin-dependent exocytosis by immature outer hair cells. J. Neurosci. *28*, 1798–1803. https://doi.org/10.1523/JNEUROSCI.4653-07.2008.

Bok, J., Zenczak, C., Hwang, C.H., and Wu, D.K. (2013). Auditory ganglion source of Sonic hedgehog regulates timing of cell cycle exit and differentiation of mammalian cochlear hair cells. Proc. Natl. Acad. Sci. USA *110*, 13869–13874. https://doi.org/10.1073/pnas.1222341110.

Bramhall, N.F., Shi, F., Arnold, K., Hochedlinger, K., and Edge, A.S.B. (2014). Lgr5-positive supporting cells generate new hair cells in the postnatal cochlea. Stem Cell Rep. *2*, 311–322. https://doi.org/10.1016/j.stemcr.2014.01.008.

Chai, R., Kuo, B., Wang, T., Liaw, E.J., Xia, A., Jan, T.A., Liu, Z., Taketo, M.M., Oghalai, J.S., Nusse, R., et al. (2012). Wnt signaling induces proliferation of sensory precursors in the postnatal mouse cochlea. Proc. Natl. Acad. Sci. USA *109*, 8167–8172. https://doi.org/10.1073/pnas.1202774109.

Chow, L.M.L., Tian, Y., Weber, T., Corbett, M., Zuo, J., and Baker, S.J. (2006). Inducible Cre recombinase activity in mouse cerebellar granule cell precursors and inner ear hair cells. Dev. Dyn. *235*, 2991–2998. https://doi.org/10.1002/dvdy.20948.

Coate, T.M., Spita, N.A., Zhang, K.D., Isgrig, K.T., and Kelley, M.W. (2015). Neuropilin-2/Semaphorin-3F-mediated repulsion promotes inner hair cell innervation by spiral ganglion neurons. Elife *4*, e07830. https://doi.org/10.7554/eLife.07830.

Cox, B.C., Chai, R., Lenoir, A., Liu, Z., Zhang, L., Nguyen, D.H., Chalasani, K., Steigelman, K.A., Fang, J., Rubel, E.W., et al. (2014). Spontaneous hair cell regeneration in the neonatal mouse cochlea in vivo. Development *141*, 816–829. https://doi.org/10.1242/dev.103036.

Defourny, J., Poirrier, A.L., Lallemend, F., Mateo Sánchez, S., Neef, J., Vanderhaeghen, P., Soriano, E., Peuckert, C., Kullander, K., Fritzsch, B., et al. (2013). Ephrin-A5/EphA4 signalling controls specific afferent targeting to cochlear hair cells. Nat. Commun. *4*, 1438. https://doi.org/10.1038/ncomms2445.

Giandomenico, S.L., Mierau, S.B., Gibbons, G.M., Wenger, L.M.D., Masullo, L., Sit, T., Sutcliffe, M., Boulanger, J., Tripodi, M., Derivery, E., et al. (2019). Cerebral organoids at the air-liquid interface generate diverse nerve tracts with functional output. Nat. Neurosci. *22*, 669–679. https://doi.org/10.1038/s41593-019-0350-2.

Gnedeva, K., and Hudspeth, A.J. (2015). SoxC transcription factors are essential for the development of the inner ear. Proc. Natl. Acad. Sci. USA *112*, 14066–14071. https://doi.org/10.1073/pnas.1517371112.

Gnedeva, K., Wang, X., McGovern, M.M., Barton, M., Tao, L., Trecek, T., Monroe, T.O., Llamas, J., Makmura, W., Martin, J.F., et al. (2020). Organ of Corti size is governed by Yap/Tead-mediated progenitor self-renewal. Proc. Natl. Acad. Sci. USA *117*, 13552–13561. https://doi.org/10.1073/pnas.2000175117.

Golub, J.S., Tong, L., Ngyuen, T.B., Hume, C.R., Palmiter, R.D., Rubel, E.W., and Stone, J.S. (2012). Hair cell replacement in adult mouse utricles after targeted ablation of hair cells with diphtheria

toxin. J. Neurosci. *32*, 15093–15105. https://doi.org/10.1523/JNEUROSCI.1709-12.2012.

Helms, A.W., Abney, A.L., Ben-Arie, N., Zoghbi, H.Y., and Johnson, J.E. (2000). Autoregulation and multiple enhancers control Math1 expression in the developing nervous system. Development *127*, 1185–1196.

Homan, K.A., Gupta, N., Kroll, K.T., Kolesky, D.B., Skylar-Scott, M., Miyoshi, T., Mau, D., Valerius, M.T., Ferrante, T., Bonventre, J.V., et al. (2019). Flow-enhanced vascularization and maturation of kidney organoids in vitro. Nat. Methods *16*, 255–262. https://doi.org/10.1038/s41592-019-0325-y.

Huch, M., Gehart, H., van Boxtel, R., Hamer, K., Blokzijl, F., Verstegen, M.M.A., Ellis, E., van Wenum, M., Fuchs, S.A., de Ligt, J., et al. (2015). Long-term culture of genome-stable bipotent stem cells from adult human liver. Cell *160*, 299–312. https://doi.org/10.1016/j.cell.2014.11.050.

Jeng, J.Y., Ceriani, F., Hendry, A., Johnson, S.L., Yen, P., Simmons, D.D., Kros, C.J., and Marcotti, W. (2020). Hair cell maturation is differentially regulated along the tonotopic axis of the mammalian cochlea. J. Physiol. *598*, 151–170. https://doi.org/10.1113/JP279012.

Johnson, S.L., Franz, C., Knipper, M., and Marcotti, W. (2009). Functional maturation of the exocytotic machinery at gerbil hair cell ribbon synapses. J. Physiol. *587*, 1715–1726. https://doi.org/10.1113/jphysiol.2009.168542.

Koehler, K.R., Mikosz, A.M., Molosh, A.I., Patel, D., and Hashino, E. (2013). Generation of inner ear sensory epithelia from pluripotent stem cells in 3D culture. Nature *500*, 217–221. https://doi.org/10.1038/nature12298.

Koehler, K.R., Nie, J., Longworth-Mills, E., Liu, X.P., Lee, J., Holt, J.R., and Hashino, E. (2017). Generation of inner ear organoids containing functional hair cells from human pluripotent stem cells. Nat. Biotechnol. *35*, 583–589. https://doi.org/10.1038/nbt.3840.

Kolla, L., Kelly, M.C., Mann, Z.F., Anaya-Rocha, A., Ellis, K., Lemons, A., Palermo, A.T., So, K.S., Mays, J.C., Orvis, J., et al. (2020). Characterization of the development of the mouse cochlear epithelium at the single cell level. Nat. Commun. *11*, 2389. https://doi.org/10.1038/s41467-020-16113-y.

Kubota, M., Scheibinger, M., Jan, T.A., and Heller, S. (2021). Greater epithelial ridge cells are the principal organoid-forming progenitors of the mouse cochlea. Cell Rep. *34*, 108646. https://doi.org/10.1016/j.celrep.2020.108646.

Lancaster, M.A., Renner, M., Martin, C.A., Wenzel, D., Bicknell, L.S., Hurles, M.E., Homfray, T., Penninger, J.M., Jackson, A.P., and Knoblich, J.A. (2013). Cerebral organoids model human brain development and microcephaly. Nature *501*, 373–379. https://doi.org/10.1038/nature12517.

Li, C., Shu, Y., Wang, G., Zhang, H., Lu, Y., Li, X., Li, G., Song, L., and Liu, Z. (2018). Characterizing a novel vGlut3-P2A-iCreER knockin mouse strain in cochlea. Hear. Res. *364*, 12–24. https://doi.org/10.1016/j.heares.2018.04.006.

Li, H., Corrales, C.E., Wang, Z., Zhao, Y., Wang, Y., Liu, H., and Heller, S. (2005). BMP4 signaling is involved in the generation of inner ear sensory epithelia. BMC Dev. Biol. *5*, 16. https://doi.org/10.1186/1471-213X-5-16.

Li, H., Liu, H., and Heller, S. (2003). Pluripotent stem cells from the adult mouse inner ear. Nat. Med. *9*, 1293–1299. https://doi.org/10.1038/nm925.

Li, W., Wu, J., Yang, J., Sun, S., Chai, R., Chen, Z.Y., and Li, H. (2015). Notch inhibition induces mitotically generated hair cells in mammalian cochleae via activating the Wnt pathway. Proc. Natl. Acad. Sci. USA *112*, 166–171. https://doi.org/10.1073/pnas.1415901112.

Liu, X.-P., Koehler, K.R., Mikosz, A.M., Hashino, E., and Holt, J.R. (2016). Functional development of mechanosensitive hair cells in stem cell-derived organoids parallels native vestibular hair cells. Nat. Commun. *7*, 11508. https://doi.org/10.1038/ncomms11508.

Low, J.H., Li, P., Chew, E.G.Y., Zhou, B., Suzuki, K., Zhang, T., Lian, M.M., Liu, M., Aizawa, E., Rodriguez Esteban, C., et al. (2019). Generation of human PSC-derived kidney organoids with patterned nephron segments and a De Novo vascular Network. Cell Stem Cell *25*, 373–387.e9. https://doi.org/10.1016/j.stem.2019.06.009.

Madisen, L., Zwingman, T.A., Sunkin, S.M., Oh, S.W., Zariwala, H.A., Gu, H., Ng, L.L., Palmiter, R.D., Hawrylycz, M.J., Jones, A.R., et al. (2010). A robust and high-throughput Cre reporting and characterization system for the whole mouse brain. Nat. Neurosci. *13*, 133–140. https://doi.org/10.1038/nn.2467.

Martinez-Monedero, R., Liu, C., Weisz, C., Vyas, P., Fuchs, P.A., and Glowatzki, E. (2016). GluA2-Containing AMPA receptors distinguish ribbon-associated from Ribbonless afferent contacts on rat cochlear hair cells. eNeuro *3*. https://doi.org/10.1523/ENEURO.0078-16.2016.

McLean, W.J., Yin, X., Lu, L., Lenz, D.R., McLean, D., Langer, R., Karp, J.M., and Edge, A.S.B. (2017). Clonal expansion of Lgr5-positive cells from mammalian cochlea and high-purity generation of sensory hair cells. Cell Rep. *18*, 1917–1929. https://doi.org/10.1016/j.celrep.2017.01.066.

Montcouquiol, M., and Kelley, M.W. (2020). Development and patterning of the cochlea: from convergent extension to planar polarity. Cold Spring Harb. Perspect. Med. *10*, a033266. https://doi.org/10.1101/cshperspect.a033266.

Munnamalai, V., Sienknecht, U.J., Duncan, R.K., Scott, M.K., Thawani, A., Fantetti, K.N., Atallah, N.M., Biesemeier, D.J., Song, K.H., Luethy, K., et al. (2017). Wnt9a can influence cell fates and neural connectivity across the radial Axis of the developing cochlea. J. Neurosci. *37*, 8975–8988. https://doi.org/10.1523/JNEUROSCI.1554-17.2017.

Nichane, M., Javed, A., Sivakamasundari, V., Ganesan, M., Ang, L.T., Kraus, P., Lufkin, T., Loh, K.M., and Lim, B. (2017). Isolation and 3D expansion of multipotent Sox9(+) mouse lung progenitors. Nat. Methods *14*, 1205–1212. https://doi.org/10.1038/nmeth.4498.

Oliver, D., Plinkert, P., Zenner, H.P., and Ruppersberg, J.P. (1997). Sodium current expression during postnatal development of rat outer hair cells. Pflugers Arch. *434*, 772–778. https://doi.org/10.1007/s004240050464.

Postigo, A., Calella, A.M., Fritzsch, B., Knipper, M., Katz, D., Eilers, A., Schimmang, T., Lewin, G.R., Klein, R., and Minichiello, L.

(2002). Distinct requirements for TrkB and TrkC signaling in target innervation by sensory neurons. Genes Dev. *16*, 633–645. https://doi.org/10.1101/gad.217902.

Ranum, P.T., Goodwin, A.T., Yoshimura, H., Kolbe, D.L., Walls, W.D., Koh, J.Y., He, D.Z.Z., and Smith, R.J.H. (2019). Insights into the biology of hearing and deafness revealed by single-cell RNA sequencing. Cell Rep. *26*, 3160–3171.e3. https://doi.org/10.1016/j.celrep.2019.02.053.

Roccio, M., Perny, M., Ealy, M., Widmer, H.R., Heller, S., and Senn, P. (2018). Molecular characterization and prospective isolation of human fetal cochlear hair cell progenitors. Nat. Commun. *9*, 4027. https://doi.org/10.1038/s41467-018-06334-7.

Ruben, R.J. (1967). Development of the inner ear of the mouse: a radioautographic study of terminal mitoses. Acta Otolaryngol. *Suppl 220*, 221–244.

Safieddine, S., El-Amraoui, A., and Petit, C. (2012). The auditory hair cell ribbon synapse: from assembly to function. Annu. Rev. Neurosci. *35*, 509–528. https://doi.org/10.1146/annurev-neuro-061010-113705.

Shearer, A.E., Hildebrand, M.S., Sloan, C.M., and Smith, R.J.H. (2011). Deafness in the genomics era. Hear. Res. *282*, 1–9. https://doi.org/10.1016/j.heares.2011.10.001.

Shi, F., Kempfle, J.S., and Edge, A.S.B. (2012). Wnt-responsive Lgr5-expressing stem cells are hair cell progenitors in the cochlea. J. Neurosci. *32*, 9639–9648. https://doi.org/10.1523/JNEUROSCI.1064-12.2012.

Sun, Y., Wu, Q., Dai, K., You, Y., and Jiang, W. (2021). Generating 3D-cultured organoids for pre-clinical modeling and treatment of degenerative joint disease. Signal Transduct. Target. Ther. *6*, 380. https://doi.org/10.1038/s41392-021-00675-4.

Tao, T., Deng, P., Wang, Y., Zhang, X., Guo, Y., Chen, W., and Qin, J. (2022). Microengineered multi-organoid system from hiPSCs to recapitulate human liver-islet Axis in normal and type 2 diabetes. Adv. Sci. *9*, e2103495. https://doi.org/10.1002/advs.202103495.

Tilney, L.G., Tilney, M.S., and DeRosier, D.J. (1992). Actin filaments, stereocilia, and hair cells: how cells count and measure. Annu. Rev. Cell Biol. *8*, 257–274. https://doi.org/10.1146/annurev.cb.08.110192.001353.

Wan, G., Gómez-Casati, M.E., Gigliello, A.R., Liberman, M.C., and Corfas, G. (2014). Neurotrophin-3 regulates ribbon synapse density in the cochlea and induces synapse regeneration after acoustic trauma. Elife *3*, e03564. https://doi.org/10.7554/eLife.03564.

Wang, B., Wu, H., Hu, C., Wang, H., Liu, J., Wang, W., and Liu, Q. (2021). An overview of kinase downregulators and recent advances in discovery approaches. Signal Transduct. Target. Ther. *6*, 423. https://doi.org/10.1038/s41392-021-00826-7.

Watanabe, K., Ueno, M., Kamiya, D., Nishiyama, A., Matsumura, M., Wataya, T., Takahashi, J.B., Nishikawa, S.i., Nishikawa, S., Muguruma, K., and Sasai, Y. (2007). A ROCK inhibitor permits survival of dissociated human embryonic stem cells. Nat. Biotechnol. *25*, 681–686. https://doi.org/10.1038/nbt1310.

Wu, H., Uchimura, K., Donnelly, E.L., Kirita, Y., Morris, S.A., and Humphreys, B.D. (2018). Comparative analysis and refinement of human PSC-derived kidney organoid differentiation with single-cell transcriptomics. Cell Stem Cell *23*, 869–881.e8. https://doi.org/10.1016/j.stem.2018.10.010.

Xia, M., Chen, Y., He, Y., Li, H., and Li, W. (2020). Activation of the RhoA-YAP-beta-catenin signaling axis promotes the expansion of inner ear progenitor cells in 3D culture. Stem Cell. *38*, 860–874. https://doi.org/10.1002/stem.3175.

Zhu, Y., Scheibinger, M., Ellwanger, D.C., Krey, J.F., Choi, D., Kelly, R.T., Heller, S., and Barr-Gillespie, P.G. (2019). Single-cell proteomics reveals changes in expression during hair-cell development. Elife *8*, e50777. https://doi.org/10.7554/eLife.50777.

Zine, A., and Romand, R. (1996). Development of the auditory receptors of the rat: a SEM study. Brain Res. *721*, 49–58. https://doi.org/10.1016/0006-8993(96)00147-3.

Stem Cell Reports, Volume *18*

Supplemental Information

Generation of innervated cochlear organoid recapitulates early development of auditory unit

Mingyu Xia, Jiaoyao Ma, Mingxuan Wu, Luo Guo, Yan Chen, Geng-lin Li, Shan Sun, Renjie Chai, Huawei Li, and Wenyan Li

SUPPLEMENTAL FIGURES

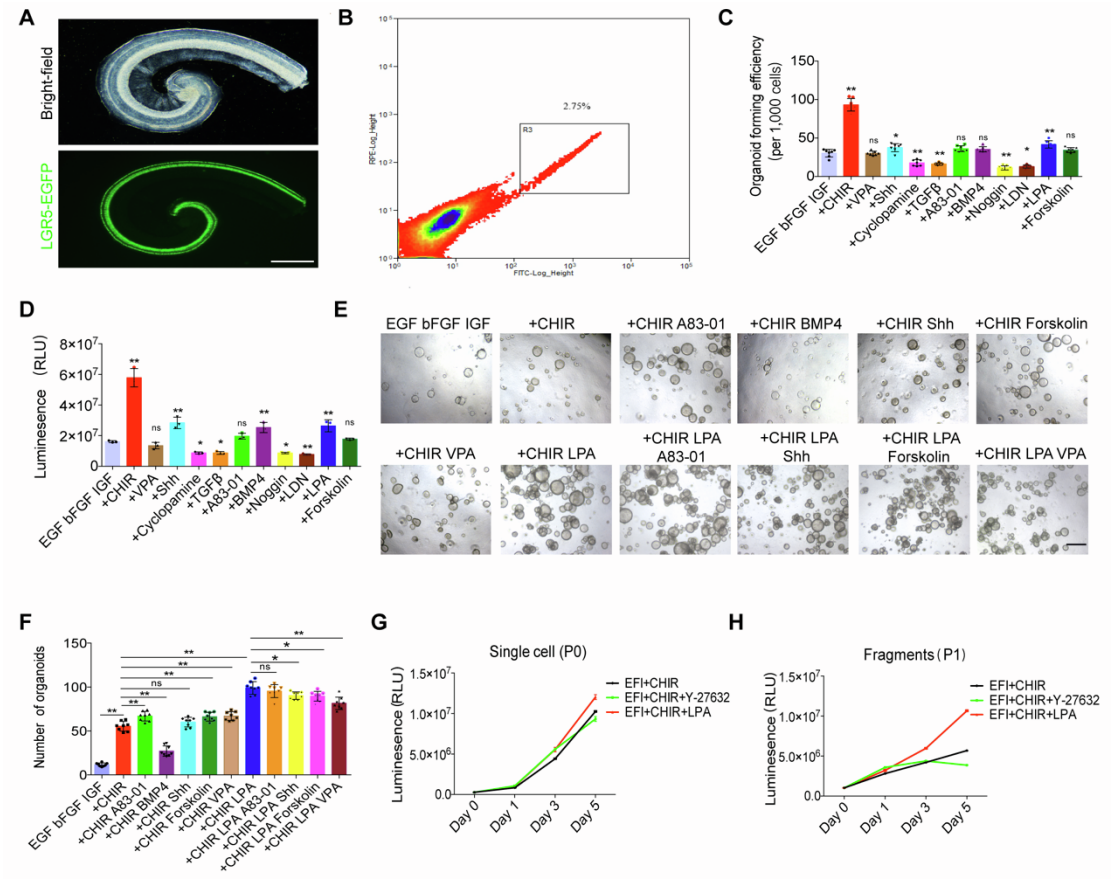

Figure S1. Screening the optimal factors for the inner ear organoid formation. (A) Bright-field and fluorescence microscopy images of the organ of Corti from a PD1 LGR5-EGFP mouse. Scale bar, 500 μm. (B) Isolate LGR5+ cochlear progenitor cells from P1 LGR5-EGFP cochleae by FACS gating strategy. (C) The efficiency of organoid formation under the indicated conditions (n = 3 independent experiments). The data are shown as means ± SEM; *P < 0.05, **P < 0.01, or nonsignificant (ns) P ≥ 0.05 (one-way ANOVA followed by Tukey's multiple comparisons test). (D) The viability of cultured organoids under the indicated conditions (n = 7 independent experiments). The data are presented as means ± SEM; *P < 0.05, **P < 0.01, or nonsignificant (ns) *P* ≥ 0.05 (one-way ANOVA followed by Tukey's multiple comparisons test). (E) Representative bright-field images of cultured P1 organoids under various combinations of growth factors. Scale bar, 500 μm. (F) The number of organoids cultured in different combinations from E (n = 8 independent experiments). The data are presented as means ± SEM; *P < 0.05, **P < 0.01, or nonsignificant (ns) P ≥ 0.05 (one-way ANOVA followed by Tukey's multiple comparisons test). (G) Growth curves of organoids from sorted single cells under the indicated conditions over 5 days (n = 6 independent experiments). (H) Growth curves of organoids from P1 fragments under the indicated conditions over 5 days (n = 6 independent experiments).

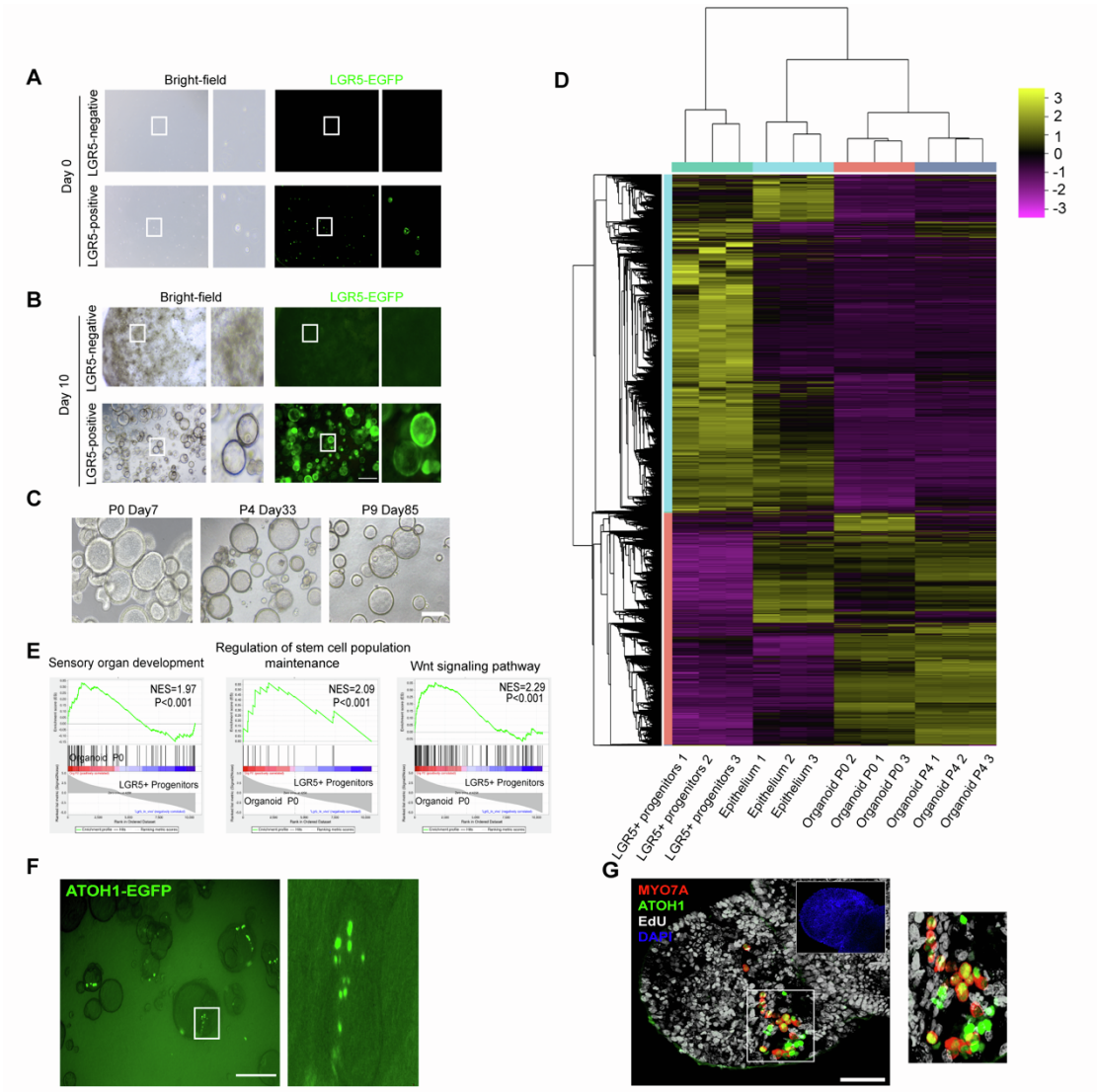

Figure S2. The transcriptome of long-term cultured cochlear organoids. (A, B) Fluorescence and bright-field images of sorted LGR5+ and LGR5– cells cultured in expansion medium at day 0 (A) and day 10 (B). Scale bar, 500 μm. (C) Bright-field images of P0, P7, and P9 organoids. Scale bar, 200 μm. (D) Heatmap showing differentially expressed genes between organoids at passage 0 and primary LGR5+ progenitor cells in the indicated cell types (n = 3). (E) GSEA of differentially expressed genes in organoids at passage 0 versus primary Lgr5+ progenitor cells (n = 3). (F) Fluorescence images showing ATOH1-EGFP expression in P0 organoids cultured in expansion medium. Scale bar, 250 μm. (G) Immunofluorescence analysis of P0 organoids showing the expression of the HC markers ATOH1 and MYO7A, with proliferative cells stained by EdU. Scale bar, 50 μm.

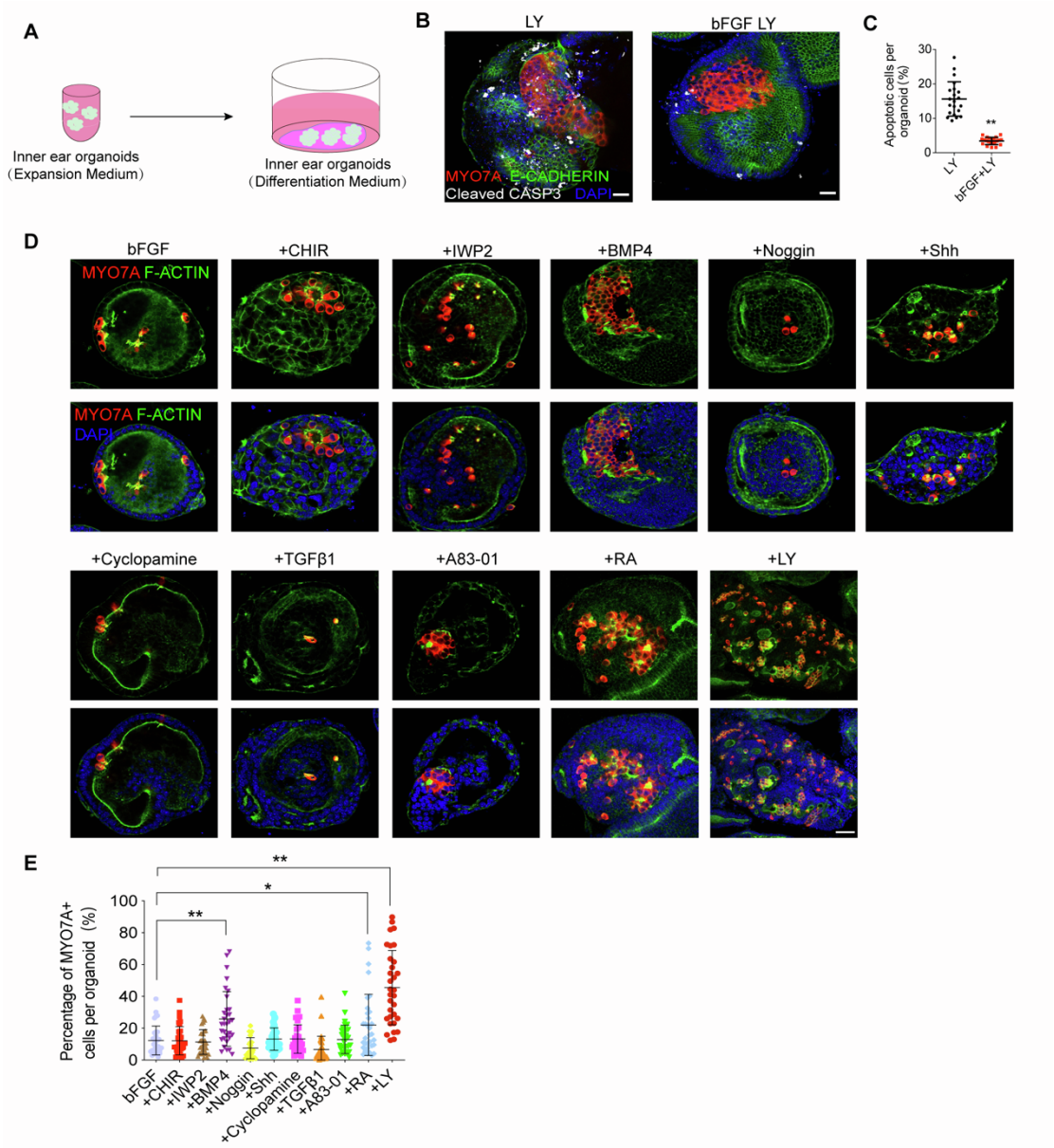

Figure S3. Screening conditions for differentiating organoids into hair cells. (A) Schematic of cochlear organoid differentiation. (B) Immunofluorescence analysis of MYO7A, E-CADHERIN, and Cleaved CASP3 expression of differentiated day 14 organoids in the indicated medium. Scale bar, 50 μm. (C) Quantify the percentage of CASP3+ apoptotic cells per organoid in the indicated medium from B. 21 organoids at each condition, three independent experiments. The data are presented as means ± SEM; ** P < 0.01 (unpaired two-tailed Student's t-test). (D) Immunofluorescence analysis of MYO7A and F-ACTIN expression of differentiated day 14 organoids in the indicated medium. Scale bar, 50 μm. (E) Quantification of the percentage of MYO7A+ cells in HC organoids. 32-33 organoids at each condition, three independent experiments. The data are presented as means ± SEM; *P < 0.05, **P < 0.01 (one-way ANOVA followed by Tukey's multiple comparisons test).

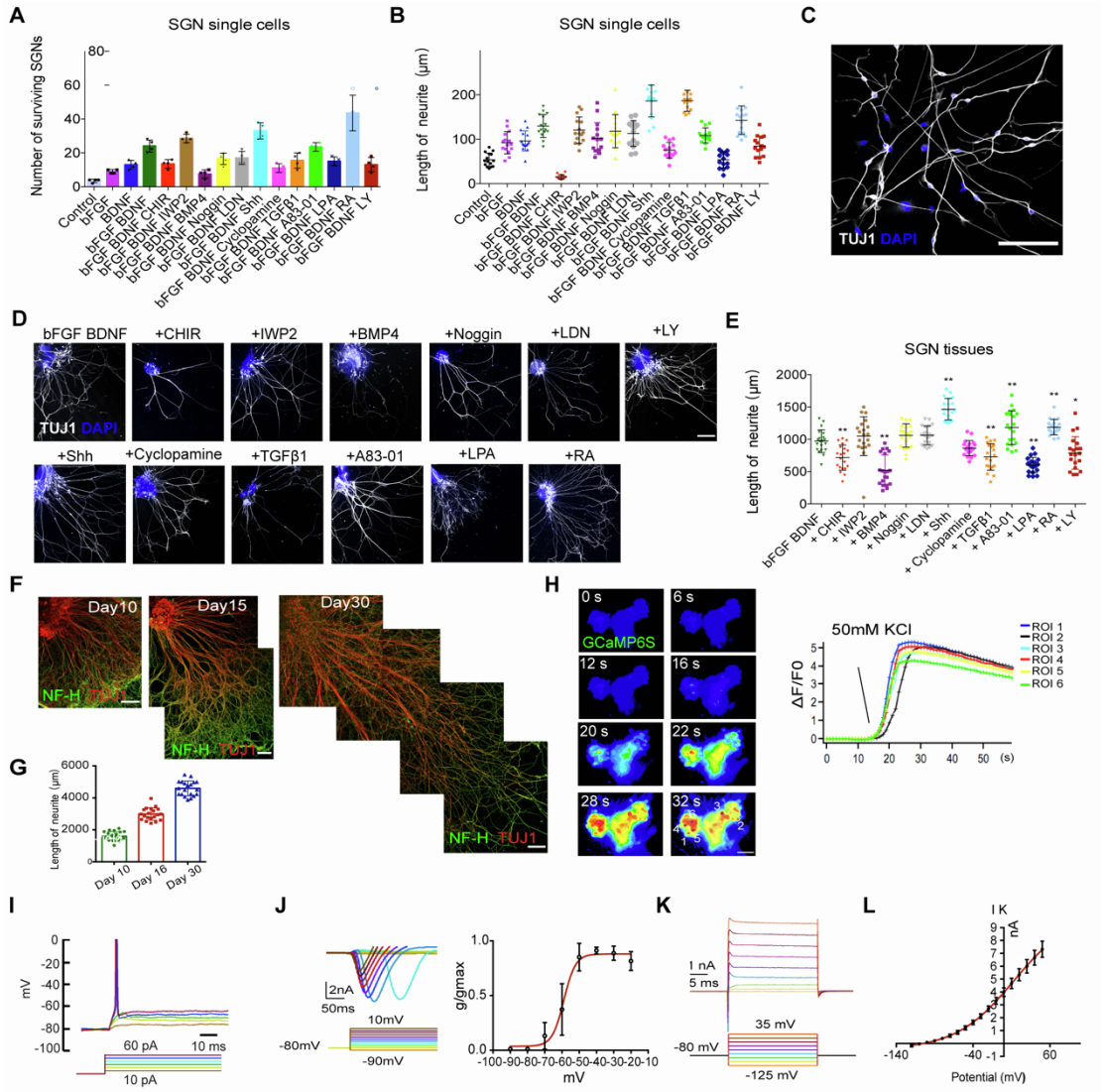

Figure S4. Screening conditions for SGN growth and Functional SGNs in co-cultures. (A) Quantify the number of SGNs cultured in different media for 7 days from dissociated single SGNs (n = 4 independent experiments). (B) Quantify the length of SGN neurites cultured in various media for 7 days from dissociated single SGNs. 15 SGNs at each stage, three independent experiments. (C) Representative fluorescence images of cultured SGNs stained with TUJ1 in the medium containing bFGF, BDNF, and Shh. Scale bar, 100 μm. (D) Immunofluorescence analysis of cultured SGN tissues in the indicated conditions at day 7 showing the staining of TUJ1. Scale bar, 300 μm. (E) Quantification of the length of SGN neurites in different media from D. 20 SGNs at each stage, three independent experiments. The data are presented as means ± SEM; *P < 0.05, **P < 0.01 (one-way ANOVA followed by Tukey's multiple comparisons test). (F) Immunofluorescence analysis of SGNs in the 3D culture at day 10, day 15, and day 30. TUJ1 staining of SGN bodies and neurites and NF-H staining of SGN neurites. Scale bar, 200 μm. (G) Quantification of the length of SGN neurites at different times from F. 20 SGNs at each stage, three independent experiments. (H) Representative image of calcium imaging in cultured day 30 SGNs and the single-cell tracings of calcium transients in the region of interest (ROI). Time is shown in seconds (s). Scale bar, 100 μm. (I) Representative images of the fired action potentials of cultured SGNs evoked by step current injections. (J) Examples of Na^+ currents of cultured SGNs elicited by voltage steps. Depolarizing voltage pulses from –90 mV to +10 mV in 10 mV steps were applied, n = 4. (K) Outward K^+ currents of cultured SGNs were elicited in response to hyperpolarizing and depolarizing voltage steps. (L) Steady-state current-voltage curves of the currents were shown in D (n = 7).

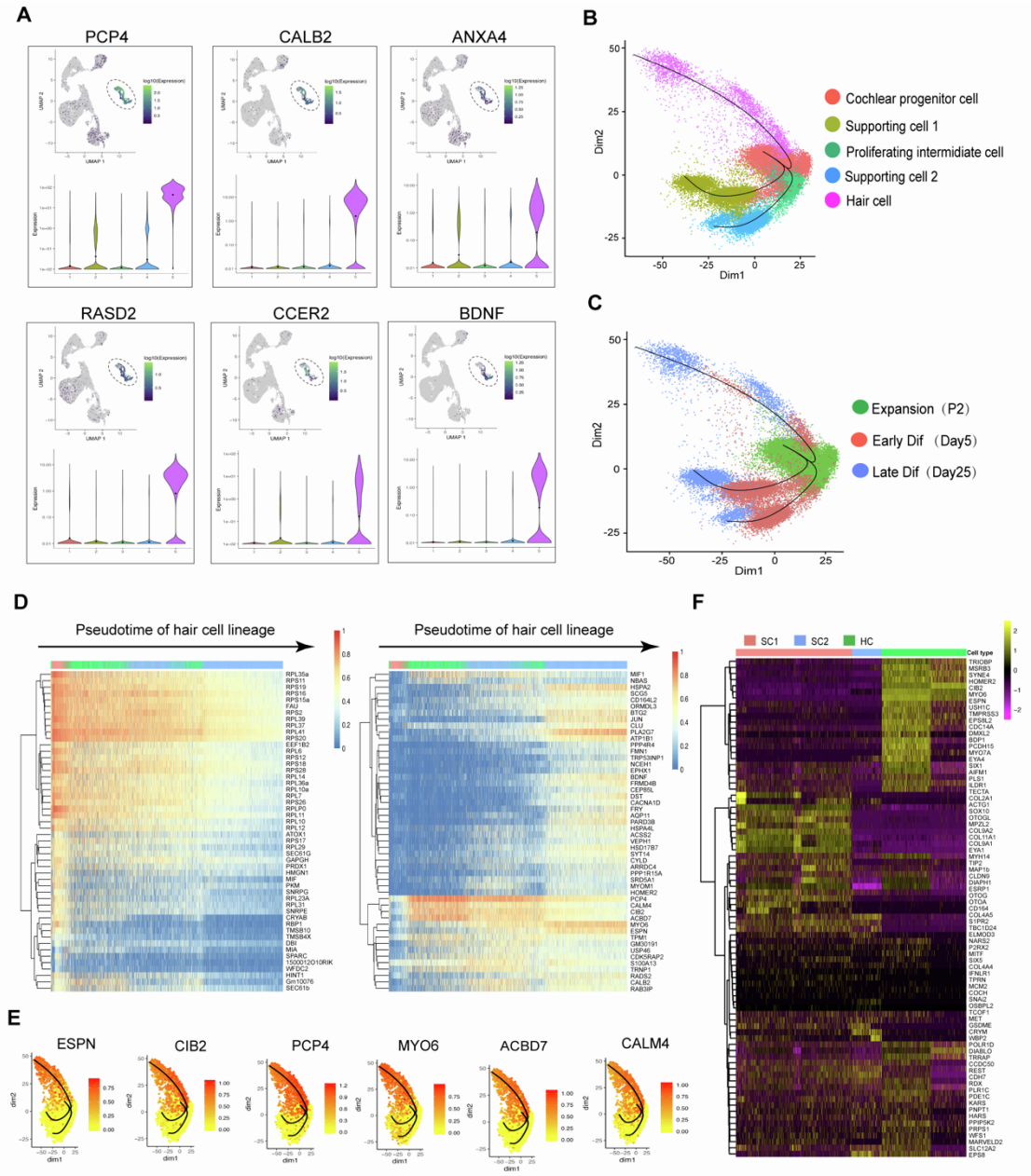

Figure S5. ScRNA-Seq analysis of HC genes during organoid development. (A) UMAP plots and violin plots show HC-related gene expression. (B, C) Pseudotime study of the five main clusters at different stages using Slingshot identified putative lineage relationships between the clusters based on gene expression similarities. Three branches were identified during organoid differentiation. (D) Heatmaps displaying the top 50 differentially expressed genes along the HC trajectory. (E) The visualizations show the lineage reconstruction color-coded by the dynamic expression of six selected genes over pseudotime. (F) Heatmap showing the expression of deafness-related genes in the SCs and HCs from differentiated day 25 organoids.

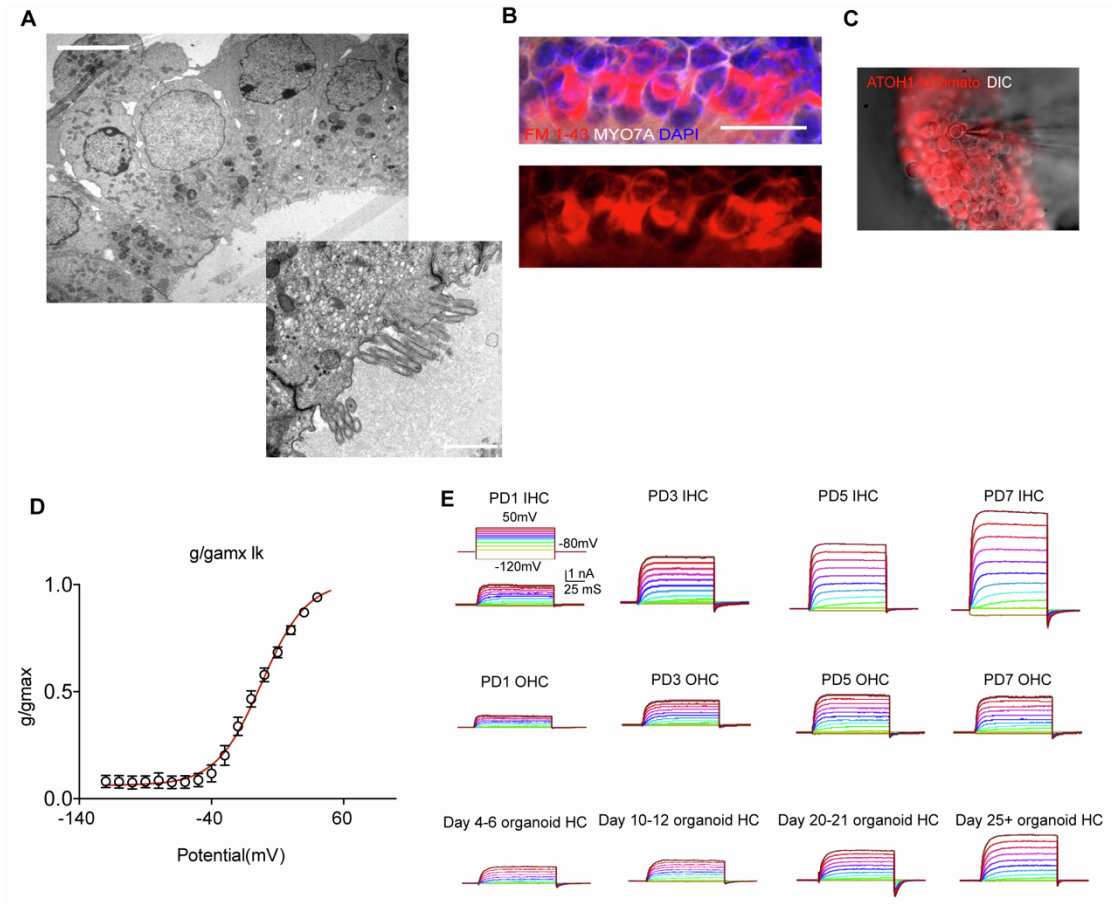

Figure S6. Characterization of differentiated HCs of cochlear organoids. (A) Transmission electron microscopy showing the ultrastructure of day30 organoid slices. Scale bar, 5 μm. Higher magnification of the images showing the stereociliary bundles of organoids. Scale bar, 1 μm. (B) Representative fluorescence analysis showing the uptake of FM1-43 dye by Myo7a+ organoid HCs. Scale bar, 25 μm. (C) Merging of DIC and fluorescence images showing recording pipettes patched to Atoh1-tdTomato+ HCs. Scale bar, 25 μm. (D) K+ currents fitted by a Boltzmann equation (line) with a half-maximal activation voltage of −50 mV in day 25 organoid HCs. (E) Examples of outward K+ currents for native HCs and organoid HCs. The stages of the HCs are indicated.

SUPPLEMENTAL TABLES

Supplemental Table 1. Primers for genotyping

Gene	Forward Primer	Reverse primer
tdTomato WT	5'-AAGGGAGCTGCAGTGGAGTA-3'	5'-CCGAAAATCTGTGGGAAGTC-3'
tdTomato Mut	5'-CTGTTCCTGTACGGCATGG-3'	5'-GGCATTAAAGCAGCGTATCC-3'
LGR5CreER WT	5'-CTGCTCTCTGCTCCCAGTCT -3'	5' - ATACCCCATCCCTTT TGAGC -3'
LGR5 CreER Mut	5'-CTGCTCTCTGCTCCCAGTCT -3'	5' - GAACTTCAGGGTCAG CTTGC -3'
POU4F3-DTR WT	5'-CACTTGGAGCGCGGAGAGCTAG-3'	5'-CCGACGGCAGCAGCTTCATGGTC-3'
POU4F3-DTR Mut	5' -GTCAAAAAAGTGCCTTAGAG -3'	5'-CCGACGGCAGCAGCTTCATGGTC-3'
ATOH1-EGFP WT	5'-GCGGTCTGGCAGTAAAAACTATC-3'	5'-GTGAAACAGCATTGCTGTCACTT-3'
ATOH1-EGFP Mut	5' -AAGTTCATCTGCACCACCG-3'	5' -TCCTTGAAGAAGATGGTGCG-3'
ATOH1 CreER WT	5'-CTAGGCCACAGAATTGAAAGATCT-3'	5'-GTAGGTGGAAATTCTAGCATCATCC-3'
ATOH1 CreER Mut	5'-GCGGTCTGGCAGTAAAAACTATC-3'	5'-GTGAAACAGCATTGCTGTCACTT-3'

Supplemental Table 2. List of antibodies and reagents

Antibodies	Supplier	Identifier
Rabbit anti-KI67	Abcam	Cat# ab15580, RRID:AB_443209
Chick anti-GFP	Abcam	Cat# ab13970, RRID:AB_300798
Chick anti-NF-H	Abcam	Cat# ab4680, RRID:AB_304560
Mouse anti-CTBP2	BD Biosciences	Cat# 612044, RRID:AB_399431
Rabbit anti-YAP	Cell Signaling Technology	Cat# 15117, RRID:AB_2798714
Cleaved CASPASE-3	Cell Signaling Technology	Cat# 9661, RRID:AB_2341188
Rabbit anti-MYO7A	Proteus BioSciences	Cat# a25-6790, RRID:AB_2314838
Mouse anti-TUJ1	Millipore	Cat# MAB5564, RRID:AB_570921
Rabbit anti-ESPIN	Novus	Cat# NBP1-90588, RRID:AB_11015490
Goat anti-PTRESIN	Santa Cruz Biotechnology	Cat# sc-22692, RRID:AB_2302038
Mouse anti-β-CATENIN	Santa Cruz Biotechnology	Cat# sc-7963, RRID:AB_626807
Goat anti-SOX2	Santa Cruz Biotechnology	Cat# SC17319, RRID:AB_661259
Rabbit anti-SOX9	Sigma	Cat# HPA001758, RRID: AB_1080067
Rabbit anti-VGLUT3	Synaptic Systems	Cat# 135 203, RRID:AB_887886
Anti-E-cadherin, Alexa Fluor 488	Thermo Fisher Scientific	Cat# 53-3249-82, RRID:AB_10671003
Mouse anti-PSD95	UC Davis/NIH NeuroMab Facility	Cat# K28/43, RRID:AB_2877189
Chemicals and recombinant proteins		
Matrigel	Corning	354230
Cell recovery solution	Corning	354253
EGF	Peprotech	315-09
bFGF	Peprotech	450-33
IGF	Peprotech	250-19
Shh	Peprotech	315-22

BMP4	Peprotech	315-27
Noggin	Peprotech	250-38
TGFβ1	R&D	P04202
Retinoic acid	Sigma	R2625
pVc	Sigma	49752
A83-01	Sigma	SML0788
Valproic acid	Sigma	PHR1061
CHIR99021	Sigma	SML1046
IWP-2	Sigma	I0536
LPA	Sigma	L7260
Y-27632	Sigma	Y0503
Forskolin	Sigma	S2449
HEPES	Sigma	PHR1428
NAC	Sigma	A9165
L-Glutamate	Sigma	G8415
NaCl	Sigma	S5886
KCl	Sigma	P5405
NaH_2PO_4	Sigma	5.43840
$CaCl_2$	Sigma	C5670
$MgCl_2$	Sigma	M4880
Dextrose	Sigma	D9434
KCH_3SO_3	Sigma	83000
EGTA	Sigma	E3889
TEA-Cl	Sigma	T2265
CsCl	Sigma	289329
Na-GTP	Sigma	G8877
Verteporfin	Sigma	SML0534
PD0325901	Sigma	PZ0162
Mg-ATP	Sigma	A9187
Cyclopamine	Selleck	S1146
SB525334	Selleck	S1476
LDN193189	Selleck	S2618
LY411575	Selleck	S2714
616452	Selleck	S7223
F-actin Readyprobes	Thermo Fisher Scientific	R37112
EdU, Alexa Fluor 647	Thermo Fisher Scientific	C10635
DMEM/F-12, GlutaMAX	Thermo Fisher Scientific	10565042
DAPI	Thermo Fisher Scientific	D1306
N-2 Supplement	Thermo Fisher Scientific	A13707
B-27 Supplement	Thermo Fisher Scientific	17504044
Penicillin-Streptomycin	Thermo Fisher Scientific	15070063
Trypsin	Thermo Fisher Scientific	25200056
Soybean Trypsin Inhibitor	Thermo Fisher Scientific	17075029
TrypLE	Thermo Fisher Scientific	12605010
FM1-43	Thermo Fisher Scientific	T35356

Supplemental Table 3. Primers for real-time PCR

Gene	Forward Primer	Reverse primer
LGR5	5'-CAGCCTCAAAGTGCTTATGCT-3'	5'-GTGGCACGTAACTGATGTGG-3'
MYO6	5'-TGTTAAGGCAGGTTCCTTGAAG-3'	5'-ACACCAGCTACAACTCGAAAC-3'
MYO7A	5' -CATCCGCCAGTACACCAACAA-3'	5' -TCCCCGCTGATAATACAGCAC-3'
POU4F3	5' -CGACGCCACCTACCATACC-3'	5' -CCCTGATGTACCGCGTGAT-3'
ACBD7	5' -ATGTCCTTGCAGGCTGATTTT-3'	5' -TGTAGAGCCCGTAGAGTTCCT-3'
CCER2	5' -AGGACCCACAAGTCTGGGG-3'	5' -CCTCCCTCTGGATGTTGCT-3'
PVALB	5' -ATCAAGAAGGCGATAGGAGCC-3'	5' -GGCCAGAAGCGTCTTTGTT-3'

SUPPLEMENTAL EXPERIMENTAL PROCEDURES

Culture of cochlear epithelia and isolation of mouse primary cochlear progenitor cells

The cochleae were dissected from postnatal day 0–1 mice and quickly placed in cold phosphate buffered saline (Hyclone). The modiolus and the stria vascularis were carefully removed to separate the sensory epithelia. The tissues were mounted on the 2 mg/ml laminin-coated glass Petri dishes for cochlear epithelial culture. After the tissues were fully attached to the dishes, the culture medium was added. To isolate cochlear progenitor cells, the tissues were incubated with 0.125% trypsin (Thermo Fisher Scientific) for 12–15 min at 37°C. An equal volume of trypsin neutralizer solution (Thermo Fisher Scientific) was added to stop the enzymatic reaction. Dissociated cells were washed with DMEM/F-12 (Thermo Fisher Scientific) twice and filtered through a 40 μm cell strainer. Cells were then resuspended in FACS buffer (2% serum, 0.2% bovine serum albumin (BSA) in DMEM/F-12 (Dulbecco's modified Eagle medium)). For sensory epithelium isolation, cells were blocked for 10 min on ice in FACS buffer before incubation with the anti-E-CADHERIN 488-conjugated antibody for 20 min. For cochlear progenitor cell isolation, cells were dissociated from LGR5-EGFP mice and then sorted using a MoFlo® SX FACS cytometer (Beckman Coulter).

Primary cochlear progenitor cell culture and expansion

Typically, sorted cells were resuspended in an expansion culture medium with a mixture of ice-cold Matrigel (Corning, 354230) at a ratio of 1:10 (vol: vol) then seeded in non-attachment plates. The expansion culture medium was based on DMEM/F-12 supplemented with penicillin/streptomycin, N2, and B27 (all from Thermo Fisher Scientific), 1.25 mM N-acetylcysteine (NAC) (Sigma), 50 ng/ml EGF (Peprotech), 50 ng/ml bFGF (Peprotech), 50 ng/ml IGF (Peprotech), 3 μM CHIR99021 (Sigma), and 10 μM Y-27632 (Sigma) on the first day. The cells were then washed with DMEM/F12 and centrifuged for 6 min at 1,500 rpm at 4°C, and the culture medium containing Y-27632 was exchanged for a medium containing 2.5 μM LPA (Sigma). Every 3–4 days, the organoids were removed from the Matrigel and culture medium by centrifugation and transferred into a new matrix. Organoids were passaged by mechanically pipetting into tiny fragments in a 1:6–1:8 split ratio every 8–10 days.

Organoid-forming efficiency and viability assays

To exclude dead cells, sorted cells were labeled by propidium iodide (Sigma) and counted using a hemocytometer. A total of 100 μl single-cell suspension (~1,000 cells) mixed with 10 μl Matrigel were plated into an ultra-low attachment U-bottom 96-well plate (corning), with each culture condition tested in triplicate. After 10 days, the number of organoids was counted. The CellTiter-Glo® 3D Cell Viability Assay (Promega) was used to test the organoid cell viability. After washing with cold PBS, the organoids were collected by centrifugation and then lysed with a CellTiter-Glo 3D kit for 15 min at room temperature. The luminescence was measured by an automatic microplate reader (Molecular Devices). EdU was supplied at a concentration of 5 μM for 4 h before fixation for labeling proliferative cells. For single-cell organoid formation, cultured cells were imaged using a Lionheart™ FX Automated Live Cell Imager and Gen5 3.03 software.

Organoid-SGN explant co-culture

For organoid differentiation, a glass Petri dish was coated with 2 mg/ml laminin solution (diluted in PBS) overnight. The organoids were subsequently transferred onto the glass dish. For culturing SGN explants, the cochlear modiolus was dissected from PD2 mice, cut into pieces without the peripheral tissue, and then plated onto the laminin-coated glass dish. To establish the periphery auditory circuit model, the SGN tissues were placed flat on the dish with the fibers facing towards the organoids, ensuring that the distance between the organoids and SGN tissues was approximately 100–300 μm. After fully adhering to the plate, 60 μl Matrigel was added to cover the organoids and SGN tissues. The differentiation medium was DMEM/F-12 supplemented with penicillin/streptomycin, N2, and B27 (all from Thermo Fisher Scientific), 1.25 mM NAC (Sigma), 10 ng/ml bFGF (Poprotech), 100 ng/ml BDNF (Poprotech), 100 ng/ml Shh (Poprotech), 0.5 μM A83-01 (Sigma), 1 μM RA (Sigma), and 5 μM LY411575 (Sigma). After 5 days of culture, the medium was exchanged to LY411575-free medium on the basis of other ingredients. After Matrigel solidification at 37°C for 30 min, the differentiation medium was added. During culture, the medium was replaced every 2–3 days.

Immunofluorescence analysis and quantification

The cultured organoids in the expansion medium were collected by centrifugation and fixed with 4% paraformaldehyde (PFA) (Sigma) on ice for 30 minutes and then centrifuged at 600 rpm for 5 minutes. After washing with PBS three times, the organoids were attached to the microscope slides by drying. For differentiated organoids, cultured SGN explants and cochlear organoid-SGN co-cultures were fixed with 4% PFA on ice overnight, then washed with PBS three times. Subsequently, the samples were permeabilized and blocked in PBS containing 1% Triton X-100 (Sigma) and 5% fetal bovine serum (Sigma) for 3 h at room temperature (RT). After incubating with primary antibodies diluted in PBS + 0.1% Triton X-100 in a humidified chamber overnight and rinsing with PBS, the samples were incubated with Alexa Fluor-conjugated secondary antibodies (1:400 diluted in PBS + 1% Triton X-100, Invitrogen) for 6 h at RT. For F-ACTIN staining, the samples were washed three times, and an Alexa 555-conjugated F-actin probe (1: 1,000 dilution, Thermo Fisher Scientific) was incubated with the samples for 15 min at RT. The Click-iT cell proliferation kit (Invitrogen) was used to visualize the EdU signal. The antibodies and relevant reagents are listed in Supplementary Table 2. After three washes in PBS, the nuclei of the samples were stained with DAPI (Sigma) for 10 min at RT. *Z*-stacks of optical sections were captured on an Sp8 confocal microscope (Leica) and processed with Fiji. Quantification of the percentage of positively stained cells was manually determined with Fiji.

In situ hybridization assays

Cochleae were isolated from P1 mice and fixed in 4% PFA for 6 h at room temperature. After washing with PBS, the samples were incubated with a gradient of sucrose solutions (15%, 20%, and 30%) and embedded in an Optimal Cutting Temperature compound (Sakura Finetek) for 2 h before flash freezing in a liquid nitrogen bath. Serial sections of the inner ear vestibular organ, cochlea, and spiral ganglion were cut at 15 μm thickness with a cryostat (Leica CM 1950). Superfrost-plus microscope slides (Thermo Scientific) were used for in situ hybridization staining of the cryosections. All samples and cryosections were stored at –80°C for no longer than 3 months before use.

RNAscope® Fluorescent Multiplex Reagents Kit, RNAscope® H2O2 and Protease Reagents Kit, RNAscope® Wash Buffer Reagents Kit, and gene-specific probes (CCER2; ACBD7) were purchased from Advanced Cell Diagnostics. In situ hybridization for CCER2 and ACBD7 was performed according to the manufacturer's protocol. The cryosections were heated at 60°C for 2 h, followed by gradient ethanol dehydration (50%, 70%, 100%, 5 min each). Sections were then immersed in H_2O_2 for 10 min at RT and pretreated with Target Retrieval Reagent (Advanced Cell Diagnostics) at 95°C for 5 min, cleared in 100% ethanol, air dried, and incubated with Protease III for 30 min at 40°C. For probe hybridization, sections were incubated with CCER2 and ACBD7 probes separately for 2 h at 40°C, and the signals were serially amplified by AMP1 to AMP3 incubation. After the addition of horseradish peroxidase (HRP), the probe signals were visualized by Opal 570 dye incubation for 30 min at 40°C, followed by HRP blocker treatment. Subsequent immunofluorescence staining was conducted using standard protocols. Images were captured on an Sp8 confocal microscope and analyzed using Fiji software.

Electron microscopy

Cochlear organoids at differentiated day6, day12, and day30 were fixed in 2.5% glutaraldehyde and 2% PFA diluted in 0.1 M phosphate buffer (PB) overnight. For scanning electron microscopy, samples were dehydrated in an ethanol gradient after washing in PB. The samples were then washed with solution A (100% ethanol + n-pentyl acetate, 2:1) and solution B (100% ethanol + n-pentyl acetate, 1:2) for 15 minutes each and then treated with 100% n-pentyl acetate for 15 min three times. After drying for 2 h, the samples were placed in the ion sputtering apparatus and sprayed with gold. Samples were analyzed using a HITACHI-H500 scanning electron microscope. For transmission electron microscopy, fixed organoids were embedded in epoxy resin (Sigma), then sectioned at a thickness of 50 nm and mounted on copper grids. Sections were stained with 4% uranyl acetate for 5 min and 0.4% lead citrate for 1 min. The ultrastructure of the stained sections was analyzed with a transmission electron microscope (CM120, Philips).

RNA isolation and quantitative real-time PCR analysis

Organoids in cocultures were picked and washed with cold PBS and centrifuged to remove the Matrigel. A RNeasy Micro Kit (Qiagen) was used to extract the total RNA from the cultured organoids, and a PrimeScript™ RT reagent Kit with gDNA Eraser kit (TaKaRa) was used to remove genomic DNA, and cDNA was synthesized according to the manufacturer's instructions. real-time PCR was performed using the TB Green *Premix Ex Taq*™ (Tli RNaseH Plus) kit (TaKaRa) on an Applied Biosystems 7500 Fast Dx Real-Time PCR Instrument. Primers for real-time PCR were designed using NCBI Primer-BLAST and are listed in Supplementary Table 3. Data were normalized to the *Gapdh* housekeeping gene, and $2^{-\Delta\Delta CT}$ values calculated relative to the appropriate control groups are shown.

RNA sequencing and analysis

Organoids cultured in the basic medium (EFG, bFGF, IGF), the basic medium + CHIR, and the basic medium + CHIR + LPA were collected, and passage 0 and passage 4 organoids in the expansion medium were collected. CPCs and cochlear epithelial cells from PD1 mice were sorted by Lgr5-EGFP and anti-E-cadherin 488-conjugated antibody staining, respectively. The RNA-sequencing libraries were generated by the Illumina mRNA-Seq Sample Prep Kit. FASTQ files of paired-end read files were generated using the SMART-Seq v4 Ultra Low Input RNA Kit for Sequencing on an Illumina HiSeq2500 150-bp Paired-End Platform. Kallisto and DEseq2 were used to analyze the RNA-seq data. Genes and transcripts were annotated using the RefGene database (NCBI). Briefly, after Benjamini–Hochberg correction for multi-testing, genes with a P-value greater than the false discovery rate were considered to be significantly differentially expressed. Differential gene expression analysis was performed with the DESeq2 package, and heatmaps were generated with the color range scaled to reflect the quantile distribution of the data. Correlation analysis was performed with the Corrplot package.

Single-cell sequencing and analysis

Organoids from passage 2 (day 8) in expansion medium, differentiated day 5, and differentiated day 25 were collected and incubated with 0.125% trypsin for 25 minutes and dissociated into single cells by mechanical pipetting. Cells were incubated with E-cadherin antibody for 10 minutes and then were stained with DAPI (Sigma) on ice for 5 minutes, and then cells were sorted using a MoFlo® SX FACS cytometer (Beckman Coulter). Sorted single, living cells were resuspended in 40 mL of fresh cell media. According to the manufacturer's recommendations, the single-cell transcriptomic profiling was performed using the Single Cell 3' Reagent v3 kits (10X Genomics). In brief, single cells were loaded on a 10X Genomics Chromium Single Cell instrument to generate single-cell gel beads in the emulsion. We used microfluidics to ensure that an individual gel bead encapsulated a single cell in an oil suspension. Gel beads in the emulsion were lysed, and RNA was reverse transcribed to cDNA followed by Illumina bridge amplification of cDNA. Libraries were sequenced on an Illumina HiSeq 4000.

Raw 10X single-cell RNA-seq data from three time points (expansion, early differentiation, and late differentiation) were demultiplexed, aligned (GRCm38), and feature-counted by Cellranger using the default settings. Downstream analysis was performed with a set of R (3.6) packages. The expression matrices were then filtered to retain cells with at least 500 genes detected and to retain genes detected in more than 1% of all cells in each dataset. The filtered matrices were combined, dimensionally reduced (monocle3 'preprocess_cds'), aligned (monocle3 'align_cds'), and clustered (resolution equals to 1×10^{-6}). The top 100 marker genes were computed for each cluster using the regression-based differential expression testing implemented in monocle3. GO term analysis was performed using ClusterProfiler, and pseudotime analysis for CPC differentiation was performed with Slingshot for the pseudotime trajectory construction and with TradeSeq for the gene expression analysis along the trajectory. The top two principal component coordinates were used as the dimension-reduction input for Slingshot, and default parameters were applied. The top genes associated with pseudotime were calculated with the TradeSeq 'startVsEndTest' function to obtain Wald statistics for each gene in each trajectory. To construct pseudotime trajectory for HC development, Monocle2 was applied. The cells were ordered by density peak clustering based on the genes differentially expressed between clusters. Data visualization for this study was performed using R packages, including monocle3, Seurat V3, TradeSeq, and heatmap.

Optogenetic stimulation and electrophysiological recordings

The AAV DJ carrying the coding sequences for Scarlet and Chrimson driven by the CAG promoter was generated using a virus-free helper system. Titers were calculated by qPCR with WPRE primers (WPRE-F: gactggtattcttaactatgttgctc; WPRE-R: ccaggatttatacaaggaggag). SGN tissues were plated in a 100 µl differentiation medium in a glass Petri dish, and 2 µl AAV was added to each well. After 24 h, the solution was exchanged entirely with a fresh medium.

The ion channel activities of infected SGNs (post-infection day 15) were tested under light stimulation. All optogenetic stimulation of Chrimson was performed with multi-wavelength LEDs mounted on the microscope (Thorlabs, LED4D241). The samples' localization and stimulating cells' selection was made under a C11440-42U30 Hamamatsu Flash 4.0 Scmos camera. Light at 5 mW/mm^2 at 590 nm was used to induce Chrimson-mediated optical spiking.

Whole-cell patch-clamp recordings were performed to measure the electrophysiological properties of cultured SGNs and organoids. To record K^+ channel and action potentials, SGNs, organ of Corti explants, and organoids were placed in extracellular solution containing 135 mM NaCl, 5.8 mM KCl, 0.7 mM NaH_2PO_4, 1.3 mM $CaCl_2$, 0.9 mM $MgCl_2$, 5.6 mM Glucose, 10 mM HEPES, and essential amino acids and vitamins (Sigma), pH 7.4, ~310 mmol/kg. Recording pipettes were filled with intracellular solution containing 135 mM potassium methanesulfonate, 20 mM KCl, 0.5 mM Na-GTP, 3 mM Mg-ATP, 10 mM HEPES, 2 mM EGTA, and essential amino acids and vitamins (Sigma), pH 7.4, ~285 mmol/kg. To record Ca^{2+} currents, samples were bathed in extracellular solution containing 100 mM NaCl, 5.8 mM KCl, 0.7 mM NaH_2PO_4, 1.3 mM $CaCl_2$, 0.9 mM $MgCl_2$, 5.6 mM Glucose, 35 mM TEA-Cl, 10 mM HEPES, and essential amino acids and vitamins (Sigma), pH 7.4, ~310 mmol/kg. Recording pipettes were filled with intracellular solution containing 135 mM cesium methanesulfonate, 10 mM CsCl, 10 mM TEA-Cl, 0.5 mM Na-GTP, 3 mM Mg-ATP, 10 mM HEPES, 2 mM EGTA, and essential amino acids and vitamins (Sigma), pH 7.4, ~285 mmol/kg. Recordings were performed with an Axopatch 200B amplifier (Molecular Devices) at RT. Data were analyzed using pClamp 10 software (Molecular Devices).

Ca^{2+} imaging

Co-cultured SGNs at day 30 were used for Ca^{2+} imaging. SGNs were transfected with AAV2/9-hSyn-Gcamp6s for 24 h and then exchanged with a fresh medium. After 15 days, infected SGNs in the differentiation medium were used to observe Ca^{2+} activity at 488-nm excitation by a Leica DM IL LED inverted microscope. For pharmacological stimulation, time-lapse images were captured before and after treatment with 50 mM KCl solution or 50 µM L-glutamate solution (Sigma) at a 1 frame/sec speed. Fluorescent image stacks were processed and analyzed using Fiji.

Statistical analyses

Statistical differences were calculated using GraphPad Prism 6.0. The results are presented as means ± SEM, and $p < 0.05$ was considered statistically significant. Unpaired two-tailed Student's t-test was performed when two groups were analyzed. To compare multiple groups, one-way ANOVA or two-way ANOVA followed by Dunnett's multiple comparison test was performed.